Perturbative Methods in General Relativity

Daniel Eriksson

Doctoral Thesis
2008

Umeå University

Department of Physics
Umeå University
SE-90187 Umeå, Sweden

ISBN: 978-91-7264-493-9

Printed by Print & Media, Umeå 2008

Abstract

Einstein's theory of general relativity is a cornerstone in the process of gaining increased understanding about problems of gravitational nature. It can be applied to problems on the huge length scales of cosmology and as far as we know it does not break down before the Planck scale is approached. Irrespective of scale, a perturbative approach is often a very useful way to reduce the Einstein system to manageable complexity and size.

The projects included in this thesis can be divided into three subcategories. In the first category the keyword is photon-photon scattering. General relativity predicts that scattering can take place on a flat background due to the curvature of space-time caused by the photons themselves. The coupling equations and cross-section are found and a comparison with the corresponding quantum field theoretical results is done to leading order. Moreover, photon-photon scattering due to exchange of virtual electron-positron pairs is considered as an effective field theory in terms of the Heisenberg-Euler Lagrangian resulting in a possible setup for experimental detection of this phenomenon using microwave cavities. The second category of projects is related to cosmology. Here linear perturbations around a flat FRW universe with a cosmological constant are considered and the corresponding temperature variations of the cosmic microwave background radiation are found. Furthermore, cosmological models of Bianchi type V are investigated using a method based on the invariant scheme for classification of metrics by Karlhede. The final category is slowly rotating stars. Here the problem of matching a perfect fluid interior of Petrov type D to an exterior axisymmetric vacuum solution is treated perturbatively up to second order in the rotational parameter.

Included papers

I **"Possibility to measure elastic photon-photon scattering in vacuum"**
D. Eriksson , G. Brodin , M. Marklund and L. Stenflo
Phys. Rev. A **70**, 013808 (2004)

II **"C^∞ perturbations of FRW models with a cosmological constant"**
Z. Perjés , M. Vasúth , V. Czinner and D. Eriksson
Astron. Astrophys. **431**, 415-421, DOI: 10.1051/0004-6361:20041472 (2005)

III **"Tilted cosmological models of Bianchi type V"**
M. Bradley and D. Eriksson
Phys. Rev. D, **73**, 044008 (2006)

IV **"Graviton mediated photon-photon scattering in general relativity"**
G. Brodin, D. Eriksson and M. Marklund
Phys. Rev. D, **74**, 124028 (2006)

V **"Slowly rotating fluid balls of Petrov type D"**
M. Bradley, D. Eriksson, G. Fodor and I. Rácz
Phys. Rev. D, **75**, 024013 (2007)

VI **"Slowly rotating fluid balls of Petrov type D - additional results"**
D. Eriksson
To be submitted

Contents

Chapter 1

Introduction

As the title suggests, the main theme throughout this thesis is a perturbative treatment of problems in general relativity with one exception, namely paper I. This project is however related to paper IV in the sense that they both deal with photon-photon scattering processes, even though the approach here is quantum field theoretical. The problems addressed in the included papers are of very different nature, ranging from calculating the cross-section for photon-photon scattering via exchange of virtual particles to considering models of slowly rotating stars and cosmological models with certain properties. The framework used for dealing with the problems in this thesis is general relativity (GR), i.e. Einstein's theory for gravitation, which coincides with Newton's in the limit of weak fields and low velocities. The theory has been strongly supported by experimental data in the weak field regime, but less is known about the validity of the predictions of GR in more extreme situations.

1.1 General Relativity - Fundamentals

GR is a theory of gravitation that differs in many ways from the Newtonian point of view, where gravitational interaction is brought about by forces acting between massive bodies according to Newton's law. Instead Einstein introduced the concept of a four dimensional space-time with a curvature determined by the distribution of matter and energy. Particles only affected by gravitation follow the straightest possible paths in this curved space-time, called geodesics. These geodesics will appear straight locally, even though it may seem like a rollercoaster ride for a distant observer, reflecting the fact that the physics is simple only when analyzed locally. In other words an inertial frame can be chosen at each point in space-time, for which the gravitational field vanishes and the laws of special relativity are valid, but in general these frames are not globally compatible. Observers moving with respect to each other will of course have different opinions of what is going on in the system. Dealing with gravitational interaction is obviously a very complicated matter since the process involves a kind of back reaction, where space-time tells matter how to move and conversely matter tells space-time how to curve. The relation between matter distribution and curvature is given by Einstein's field equations

$$G_{ij} = \kappa T_{ij} \,,$$

where κ is a constant, T_{ij} is the energy-momentum tensor containing information about the distribution of matter and G_{ij} is the Einstein tensor describing the curvature. Due to the symmetry properties, this is a set of ten coupled second order differential equations. GR has given several accurate predictions contradicting Newtonian theory such as the bending of light passing by a massive object or the perihelion advance of the planetary orbits in our solar system. However, generally speaking the differences between GR and Newtonian theory tend to appear clearly only in extreme situations such as in the vicinity of extremely compact objects or at speeds close to the speed of light.

An important prediction by GR is the existence of gravitational waves, which is a phenomenon with no Newtonian counterpart. The idea is that accelerated masses emit gravitational waves in analogy with the the emission of electromagnetic waves associated with accelerated charges in Maxwellian theory. These gravitational waves can be thought of as propagating ripples in the curvature of space-time. The way a gravitational wave affects test particles passing through them suggests that large scale interferometry is a good method for detection. Lately considerable resources have been spent on projects of this kind, e.g. the space-based LISA [1] as well as the ground based VIRGO [2] and LIGO [3]. Gravitational waves are assumed to be an important mechanism for energy loss in binary systems of massive stars or black holes, possibly resulting in premature collapse.

The mathematical formulation of GR is based on differential geometry. Here spacetime is represented by a manifold, i.e. a set with certain properties regarding smoothness on which different geometrical objects can be placed. Each point on the manifold can be identified with a physical event. The curvature of the space-time manifold is described by the metric, which is an operator determining the distance between two nearby points. A geometry is thus described by a manifold $\mathcal{M}$ and a metric g_{ij}. The metric (and quantities derivable directly from it) is the only space-time quantity possibly appearing in the laws of physics as the principle of general covariance states.

1.2 Perturbation theory

Assume that we want to investigate the time evolution of a small density perturbation in a homogeneous cosmological model or how slow rotation changes the gravitational field of a spherically symmetric object or even how a small displacement would affect a binary system. Analyzing the Einstein system for problems of this kind shows that the number of terms as well as the complexity tends to blow up to enormous proportions. As suggested above, finding analytic solutions to problems of gravitational nature can often be a difficult task even under considerable simplifying assumptions, which motivates the following course of action. Whenever the complexity of a system of equations is overwhelming and there is a suitable known exact solution, it might be a good idea to consider small perturbations around the known solution. This is done by writing the variables A_i as a sum of a zeroth order part $A_i^{(0)}$, corresponding to the exact solution, and

a small perturbation according to

$$A_i = A_i^{(0)} + \epsilon A_i^{(1)} + \epsilon^2 A_i^{(2)} + \dots .$$

Plugging the ansatz into the system of equations and collecting terms order by order in the perturbative parameter ϵ, a simplified system can be obtained, from which information about the full system hopefully can be extracted. An important detail, when performing a perturbative analysis, is to ensure the existence of an exact solution corresponding to the solution of the linearized equations. In GR the lack of an identifiable fixed background model also implies a gauge problem. The process of perturbing a metric has no unique inverse and in general there is a certain gauge freedom in the variables describing the perturbations. Thus the solutions to the perturbative equations can in principle correspond to variation of gauge choice as well as physical variation. Consequently, it is essential to keep track of the gauge freedom, e.g. by using gauge invariant variables. More information about the gauge problem can be found in [4].

1.3 Outline

Chapter 2 is intended to give some basic understanding of quantum field theory and in particular how it changes the way we look at vacuum. The main focus is set on two non-classical photon-photon scattering processes that can take place in vacuum, namely due to exchange of virtual electron-positron pairs and via creation and annihilation of a virtual graviton. In chapter 3 the same processes are treated as nonlinear wave interactions. The former can be expressed as an effective field theory and thus the evolution is determined performing the variation of a Lagrangian density. In the other case the interaction is considered as a result of self-induced nonlinear perturbations of the gravitational background in a general relativistic context. Then the discussion takes a turn towards interaction in confined regions and the possiblity of experimental detection. Chapter 4 contains an overview of the equivalence problem in GR and a description of how the algorithm for solving this problem can be reversed to give a method for finding new solutions to Einstein's equations. This method is then in chapter 5 applied to find cosmological models of Bianchi type V, which is a subclass of spatially homogeneous, anisotropic, perfect fluid models. This chapter also includes a discussion about perturbations around the spatially homogeneous, isotropic flat Friedman universe with a cosmological constant. Finally, chapter 6 deals with a more astrophysical application of GR, namely models of slowly, rigidly rotating stars. The problem of matching the rotating interior to an exterior vacuum solution is treated perturbatively.

Chapter 2

Quantum Field Theory

In the beginning of the 20th century Planck presented the hypothesis that the emission of light by atoms occurs discontinuously in quanta. This rather revolutionizing idea was based on studies of the spectrum of black-body radiation. A few years later Einstein found, while investigating the photoelectric effect, that the electromagnetic field itself consists of quanta called photons. His conclusion turned out to be in good agreement with experimental data on the Compton effect and soon led to the natural generalization that all classical fields are quantized by different kinds of particles. Interaction between these particles is mediated by other fields and their corresponding particles. For example interaction between electrons and positrons is associated with an exchange of photons. The modern quantum field theory (QFT) is a result of trying to reconcile quantum mechanics and special relativity. A key concept here is Lorentz invariance. The Schrödinger equation governing the time evolution for a non-relativistic particle is not invariant under Lorentz transformations. Trying to solve this problem led to a number of new relativistic wave equations like the Dirac and the Klein-Gordon equation. However, it turned out that a relativistic quantum theory with a fixed number of particles is an impossibility and thus relativistic wave mechanics had to give way for quantum field theory. The line of thought and main concepts that resulted in the invention of QFT are summarized in figure 2.1.

An analytical treatment of the interaction in QFT is extremely complicated, but in the limit of weak interaction perturbation theory is a powerful tool for accurate predictions. For quantum electrodynamics, i.e. interaction between the electromagnetic and the electron-positron fields, this method has turned out to be very successful. The transition amplitudes for different processes can be evaluated perturbatively using Feynman diagrams. This method makes it possible to make predictions about complicated processes and obtain the mathematical details graphically.

Note that, despite QFT has given many accurate predictions, it is not sure by any means that it is a fundamental theory. Maybe it is just a low-energy approximation of some underlying theory like string theory.

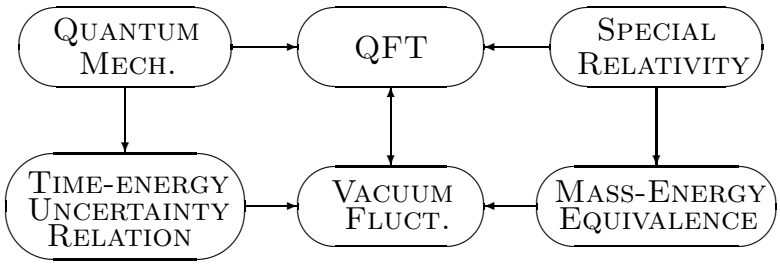

Figure 2.1: QFT is the result of an attempt to reconcile quantum mechanics and special relativity.

2.1 Quantization of the fields

In this section a very brief summary of classical Lagrangian field theory is given as a starting point. For the quantization procedure two main approaches are available, the canonical formalism due to Schrödinger, Heisenberg and Dirac emphasizing the particle-wave duality, or the path integral formulation due to Feynman and Schwinger. The equivalence of the two approaches has been shown by Feynman.

2.1.1 Classical Lagrangian field theory

Initially we consider a classical system depending on the fields $\Phi_r(x)$, where $r = 1, \ldots, N$ and $x \equiv x^\alpha$. We define a Lagrangian density $\mathcal{L} = \mathcal{L}(\Phi_r, \Phi_{r,\alpha)}$ such that variation of the action integral

$$S(\mathcal{L}) = \int_\Omega d^4x \mathcal{L}(\Phi_r, \Phi_{r,\alpha)}\,,$$

where $\Phi_{r,\alpha} \equiv \frac{\partial \Phi_r}{\partial x^\alpha}$ and Ω is some arbitrary region of the space-time, yields the equations of motion for the fields. This is not the most general case, but it is sufficient in most cases. Performing the variation

$$\Phi_r(x) \to \Phi_r(x) + \delta\Phi_r(x)$$

of the fields and requiring that $\delta S(\Omega)$ is zero in Ω and that $\delta\Phi_r$ vanishes on the boundary of Ω, we obtain the equations of motion for the fields known as the Euler-Lagrange equations

$$\frac{\partial \mathcal{L}}{\partial \Phi_r} - \frac{\partial}{\partial x^\alpha}\left(\frac{\partial \mathcal{L}}{\partial \Phi_{r,\alpha}}\right) = 0\,.$$

2.1.2 Canonical formalism

Quantization of the classical theory using the canonical formalism is done by introducing conjugate variables. The fields conjugate to $\Phi_r(x)$ are defined as

$$\pi_r(x) = \frac{\partial \mathcal{L}}{\partial \dot{\Phi}_r} ,$$

where a dot denotes derivative with respect to time. The conjugate coordinates and momenta are now interpreted as Heisenberg operators and certain commutation relations are imposed. The system has a continuously infinite number of degrees of freedom corresponding to the values of the fields at each point in space-time. In practice, when dealing with the details of this procedure, a discrete approximation of the system is used and in the end the continuum limit is considered. The continuous versions of the commutation relations are given by

$$\begin{aligned} [\Phi_r(\mathbf{x}, t), \pi_s(\mathbf{x}', t)] &= i\delta_{rs}\delta(\mathbf{x} - \mathbf{x}') , \\ [\Phi_r(\mathbf{x}, t), \Phi_s(\mathbf{x}', t)] = [\pi_r(\mathbf{x}, t), \pi_s(\mathbf{x}', t)] &= 0 . \end{aligned}$$

2.1.3 Path integral formulation

The path integral formulation is based on the following two postulates by Feynman.

- The amplitude for an event is given by adding together all the histories which include that event.
- The amplitude contribution from a certain history is proportional to $e^{\frac{i}{\hbar}S[\mathcal{L}]}$, where $S[\mathcal{L}]$ is the action of that history.

Now the total probability for a certain event can be found by summing over all possible histories leading from an initial state $|\, i\rangle$ to a final state $|\, f\rangle$. In terms of fields this can be interpreted as all possible time evolutions of the fields over all space connecting the initial and final configurations. The resulting transition amplitude is a path integral

$$\langle\, f \,|\, i\rangle = \int \mathcal{D}\Phi e^{\frac{i}{\hbar}S[\mathcal{L}]} ,$$

where $\mathcal{D}\Phi$ denotes integration over all paths. The path integral formulation is obviously very similar to the use of partition functions in statistical mechanics. After a first glance at this formulation it appears to be very abstract and of no practical use, but there are sophisticated methods available for evaluating the path integral [5]. Furthermore, it is more suitable for treating processes including non-perturbative effects.

2.2 Quantum Vacuum

In classical theory vacuum is defined very naturally as a region of spacetime containing no particles. Now let us consider how to generalize the concept of vacuum to quantum theory. A fundamental new feature in QFT mentioned above is that the number of particles of a system is allowed to change as long as certain conservation laws (energy, momentum, charge, spin etc.) are satisfied. This gives rise to several interesting new processes like scattering of real particles via creation and annihilation of virtual particles and particle-antiparticle pair creation. We will see that the latter actually causes differences between the properties of vacuum in a classical and a quantum sense. It is important to distinguish real particles from virtual, which are intermediate particles that do not have to obey the laws of energy-momentum conservation. The rapid fluctuations of virtual particles allowed by QFT suggests that the quantum definition of vacuum should be a region of spacetime containing no real particles.

2.3 Photon-Photon Scattering

In this section a short description of two photon-photon scattering processes, which are allowed in vacuum, will be given. The graviton mediated scattering is a considerably weaker effect in a major part of the frequency spectrum, but can become important in the long wavelength limit.

2.3.1 Via exchange of virtual electron-positron pairs

Vacuum fluctuations of charged particles can, even though the total charge is conserved, under the influence of an external electric field lead to an effective nonlinear polarization of vacuum. Consequently electromagnetic waves propagating in vacuum will interact and an energy transfer can occur. On a microscopic level the lowest order contribution to photon-photon scattering due to the exchange of virtual electron-positron pairs can be visualized by the Feynman diagram shown in figure 2.2. Calculating the cross-section for this kind of process shows that it is an extremely weak effect. Although several feasible proposals of detection methods have been presented in the literature recently, no successful experimental confirmation of these theoretical predictions has been made. In paper I we suggest an experimental setup for detection using microwave cavities.

Heisenberg-Euler Lagrangian

As an alternative to the microscopic description, photon-photon scattering due to the interaction with virtual electron-positron pairs can be formulated as an effective field theory in terms of the electromagnetic fields. The interaction can up to one-loop accuracy

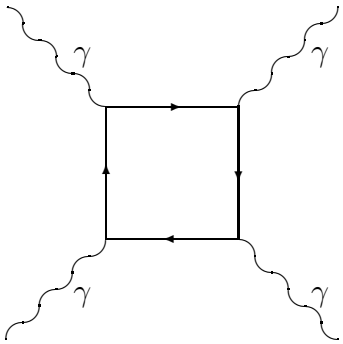

Figure 2.2: Lowest order contribution to photon-photon scattering through exchange of virtual electron-positron pairs. The solid lines with arrows represent fermions and the wavy lines photons.

be described by the Heisenberg-Euler Lagrangian which is given by

$$\mathcal{L} = \epsilon_0 F + \kappa\epsilon_0^2 \left[4F^2 + 7G^2\right], \tag{2.1}$$

where $F = (E^2 - c^2B^2)/2$, $G = c\mathbf{E}\cdot\mathbf{B}$ and $\kappa = 2\alpha^2\hbar^3/45m_e^4c^5$. Here α is the fine-structure constant, m_e the electron mass, c the velocity of light in vacuum and $\hbar$ Planck's constant. The first term can be identified as the classical Lagrangian density and thus the second represents the lowest order QED correction. The derivation of (2.1) is lengthy and will not be accounted for here, but details concerning the derivation as well as two-loop corrections can be found in [6]. The expression is valid for field strengths below the QED critical field 10^{18}V/m and wavelengths longer than the Compton wavelength 10^{-12}m.

Alternatively the photon-photon scattering can be described as nonlinear polarization and magnetization terms in Maxwell's equations. It can be shown by minimizing the action $\mathcal{S} = \int \mathcal{L}dt$ varying the vector potential amplitudes that the polarization $\mathbf{P}$ and magnetization $\mathbf{M}$ due to the vacuum fluctuations are given by

$$\begin{aligned}
\mathbf{P} &= 2\kappa\epsilon_0^2 \left[2\left(E^2 - c^2B^2\right)\mathbf{E} + 7c^2\left(\mathbf{E}\cdot\mathbf{B}\right)\mathbf{B}\right], \\
\mathbf{M} &= -2c^2\kappa\epsilon_0^2 \left[2\left(E^2 - c^2B^2\right)\mathbf{B} + 7\left(\mathbf{E}\cdot\mathbf{B}\right)\mathbf{E}\right].
\end{aligned}$$

They appear as third order source terms in the following wave equations, which can be derived from Maxwell's equations

$$\begin{aligned}
\frac{1}{c^2}\frac{\partial^2\mathbf{E}}{\partial t^2} - \nabla^2\mathbf{E} &= -\mu_0\left[\frac{\partial^2\mathbf{P}}{\partial t^2} + c^2\nabla\left(\nabla\cdot\mathbf{P}\right) + \frac{\partial}{\partial t}\left(\nabla\times\mathbf{M}\right)\right], \\
\frac{1}{c^2}\frac{\partial^2\mathbf{B}}{\partial t^2} - \nabla^2\mathbf{B} &= \mu_0\left[\nabla\times\left(\nabla\times\mathbf{M}\right) + \frac{\partial}{\partial t}\left(\nabla\times\mathbf{P}\right)\right].
\end{aligned}$$

Thus the QED effects can be treated classically using either the Lagrangian formulation or the equivalent corrections to the polarization and magnetization.

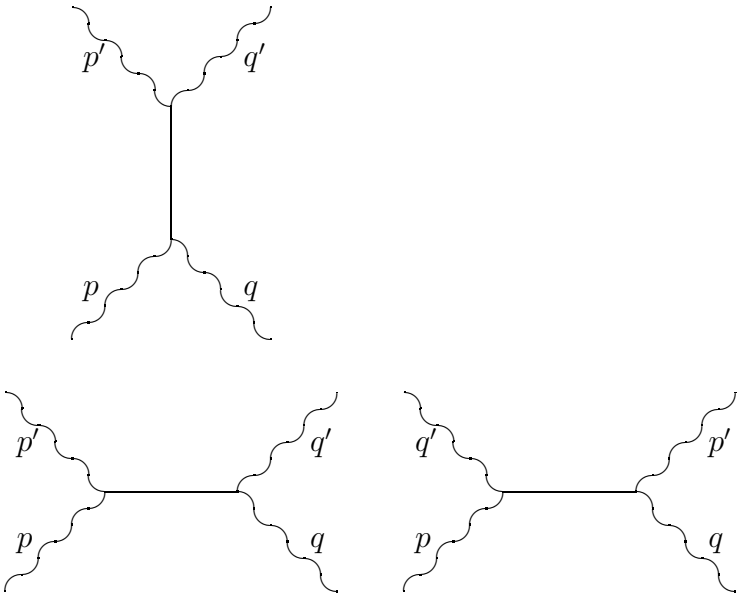

Figure 2.3: Contributions to photon-photon scattering through creation and annihilation of a graviton. The wavy lines represent photons and the solid lines gravitons.

2.3.2 Mediated by Graviton

Photons can also interact gravitationally through the creation and annihilation of a virtual graviton. The lowest order contributions are given by the three Feynman diagrams in figure 2.3. The unpolarized differential cross-section for this gravitational interaction has been calculated using quantum field theoretical methods [7] as

$$\frac{d\sigma}{d\Omega} = \frac{32G^2(h\nu)^2}{c^8 \sin^4\theta}\left[1 + (1+\sin^2(\theta/2))^2\cos^{12}(\theta/2) + (1+\cos^2(\theta/2))^2\sin^{12}(\theta/2)\right] , \quad (2.2)$$

where θ is the scattering angle and $h\nu$ is the photon energy. In paper IV we investigate whether the result is consistent with classical general relativistic calculations of photon-photon scattering via self-induced gravitational perturbations of the background metric. This matter will be further discussed in section 3.2.2.

2.3.3 Comparison betweeen the considered processes

Here we investigate the relative importance of the photon-photon scattering processes described in the previous two subsections as a function of the photon energy. Knowing the corresponding cross-sections and noting the difference in frequency dependence, it is possible to make a crude estimation of where in the frequency spectrum the contributions

become comparable. It is clear from (2.2) that the graviton mediated scattering is proportional to ω^2, while the scattering via virtual electron-positron pairs is proportional to ω^6 [8]. For frequencies higher than approximately $\omega \sim 30$ rad/s the latter turns out to be the dominant contribution.

Chapter 3

Wave Interaction

The aim of this chapter is not to give a complete description of wave interaction phenomena, but rather to give a short review of some basic concepts and methods in order to clarify papers I and IV. Sections 3.1 and 3.2 deal with the problem of finding the evolution equations for the field amplitudes for the two considered photon-photon scattering processes. The concluding sections contain a discussion concerning theoretical and experimental aspects of studying wave interaction in bounded regions. The ideas result in a concrete experimental setup for detection of photon-photon scattering due to exchange of virtual electron-positron pairs. Previous suggestions of detection schemes in the literature can be found in e.g. [9]-[17], but no successful attempt has been carried out so far.

3.1 Wave-wave interaction

Interaction between N waves denoted by ψ_1, ψ_2, ..., ψ_N can be described by a system of equations on the form

$$\hat{D}_n \psi_n = S_n(\psi_1, \psi_2, \ldots, \psi_N), \tag{3.1}$$

where $\hat{D}_n$ are the wave propagators. The interaction is called linear if all the source terms, S_i, are linear in the fields, else the interaction is called nonlinear. If the interaction is weak we can use a plane wave representation

$$\psi_n = \tilde{\psi}_n(x^\mu) e^{ik_{n\mu}x^\mu} + c.c.\,, \tag{3.2}$$

where $k_n = (\omega_n, \mathbf{k}_n)$ and the complex amplitudes $\tilde{\psi}_n$ depend weakly on space and time, i.e. $|\partial_\mu \psi_n(x^\nu)| \ll |k_\mu|\,|\psi_n(x^\nu)|$. Here $c.c$ is an abbreviation for complex conjugate of the previous term. It is clear from (3.1) and (3.2) that nonlinear wave-wave interaction produces several higher harmonics, but the most important contribution is the resonant part which is characterized by the exponential factor of the left and right hand side being equal. Resonant terms can be obtained due to certain relations between the wave vectors

and frequencies of the interacting waves called matching conditions, corresponding to conservation of energy and momentum. The non-resonant contributions can be interpreted as rapid variations in the field amplitudes, which are negligible when averaging over space and time. Note that we actually get some self-interaction terms as well, but these are of no interest for the wave coupling. Picking out the resonant terms gives time evolution equations for the field amplitudes in the form

$$\frac{\partial\tilde{\psi}_n}{\partial t} = C_n f_n(\tilde{\psi}_1, \tilde{\psi}_2, \ldots, \tilde{\psi}_{n-1}, \tilde{\psi}_{n+1}, \ldots, \tilde{\psi}_N),$$

where f_n are functions determined by the matching conditions and C_n are called coupling coefficients. Consider four wave interaction in the center of mass frame as an example. The matching conditions then read

$$k_1^\mu + k_2^\mu = k_3^\mu + k_4^\mu$$

and the waves will counterpropagate pairwise, i.e. $\mathbf{k}_1 = -\mathbf{k}_2$ and $\mathbf{k}_3 = -\mathbf{k}_4$. Consequently the resonants terms contributing to the time evolution of $\tilde{\psi}_1$ will be proportional to $\tilde{\psi}_3\tilde{\psi}_4\tilde{\psi}_2^*$.

When dealing with interaction processes where an effective field theory is available, a convenient approach to finding the evolution equations is to start out from the Lagrangian and perform the variation of the field amplitudes. This method will reduce the length of the calculations considerably compared to starting out from the wave equations. In paper I photon-photon scattering due to exchange of virtual electron-positron pairs is treated as a variation of the Heisenberg-Euler Lagrangian described in section 2.3.1. Here we have a situation where two waves act as pump modes coupling to a much weaker third frequency. Then it is a good approximation that the amplitudes of the pump modes are unaffected by the interaction. More details concerning paper I will follow at the end of this chapter.

3.2 Interaction between EM waves via self-induced gravitational perturbations

From a general relativistic point of view, waves can also interact due to nonlinearities in the geometry of the spacetime in which they are propagating. Since all matter and energy contributes to the curvature of spacetime, waves will in some sense influence their own propagation even on an otherwise flat background. In the case of electromagnetic waves this interaction is governed by the classical Einstein-Maxwell system.

3.2.1 Einstein-Maxwell system

Assume that no matter is present in addition to the electromagnetic waves. Then the total energy-momentum tensor, determining the curvature through Einstein's equations,

is given by

$$T_{ab} = F^c_a F_{bc} - \frac{1}{4} g_{ab} F^{cd} F_{cd}\,,$$

where F^{ab} is the electromagnetic field tensor. The metric perturbations can be found by making a suitable ansatz, in the optimal case being simple but still including all resonant terms, and plugging it into the field equations. This step also involves the use of the generalized Lorentz condition in order to determine all components of the metric. Via the metric perturbations the Ricci rotation coefficients can be obtained as second order quantities in the field amplitudes. From Maxwell's equations

$$\begin{aligned} \nabla_{[a} F_{bc]} &= 0\,, \\ \nabla_a F^{ab} &= j^b, \end{aligned}$$

where j^b is the four-current density (vanishing in the present case), it is possible to derive the following wave equations in an orthonormal frame $\{\mathbf{e}_a = e^{\ \mu}_a \partial_\mu\}$

$$\begin{aligned} \tilde{\Box} E^\alpha &= -\mathbf{e}_0 j^\alpha_E - \epsilon^{\alpha\beta\gamma} \mathbf{e}_\beta j_{B\gamma} - \delta^{\alpha\gamma} \mathbf{e}_\gamma \rho_E - \\ &\quad \epsilon^{\alpha\beta\gamma} C^a_{\beta 0} \mathbf{e}_a B_\gamma - \delta^{\alpha\gamma} C^a_{\beta\gamma} \mathbf{e}_a E^\beta, \qquad (3.3) \\ \tilde{\Box} B^\alpha &= -\mathbf{e}_0 j^\alpha_B + \epsilon^{\alpha\beta\gamma} \mathbf{e}_\beta j_{E\gamma} - \delta^{\alpha\gamma} \mathbf{e}_\gamma \rho_B + \\ &\quad \epsilon^{\alpha\beta\gamma} C^a_{\beta 0} \mathbf{e}_a E_\gamma - \delta^{\alpha\gamma} C^a_{\beta\gamma} \mathbf{e}_a B^\beta. \qquad (3.4) \end{aligned}$$

Here $\tilde{\Box} \equiv \mathbf{e}_0 \cdot \mathbf{e}_0 + \nabla \cdot \nabla$, $\nabla \equiv (\mathbf{e}_1, \mathbf{e}_2, \mathbf{e}_3)$, $B_\alpha = \frac{1}{2} \epsilon_{\alpha\beta\gamma\delta} F^{\beta\gamma} u^\delta$, $E_\alpha = F_{\alpha\beta} u^\beta$ and C^c_{ab} are commutation functions for the frame vectors satisfying $[\mathbf{e}_a, \mathbf{e}_b] = C^c_{ab} \mathbf{e}_c$. The gravitational coupling appears in the the effective currents and charges

$$\begin{aligned} \mathbf{j}_E &= \Big[-\left(\gamma^\alpha_{0\beta} - \gamma^\alpha_{\beta 0}\right) E^\beta + \gamma^\beta_{0\beta} E^\alpha - \epsilon^{\alpha\beta\sigma} \left(\gamma^0_{\beta 0} B_\sigma + \gamma^\delta_{\beta\sigma} B_\delta\right) \Big] \mathbf{e}_\alpha, \\ \mathbf{j}_B &= \Big[-\left(\gamma^\alpha_{0\beta} - \gamma^\alpha_{\beta 0}\right) B^\beta + \gamma^\beta_{0\beta} B^\alpha - \epsilon^{\alpha\beta\sigma} \left(\gamma^0_{\beta 0} E_\sigma + \gamma^\delta_{\beta\sigma} E_\delta\right) \Big] \mathbf{e}_\alpha, \\ \rho_E &= -\gamma^\alpha_{\beta\alpha} E^\beta - \epsilon^{\alpha\beta\sigma} \gamma^0_{\alpha\beta} B_\sigma, \\ \rho_B &= -\gamma^\alpha_{\beta\alpha} B^\beta - \epsilon^{\alpha\beta\sigma} \gamma^0_{\alpha\beta} E_\sigma, \end{aligned}$$

where γ^a_{bc} are the Ricci rotation coefficients. In the above expressions Roman tetrad indices $a, b, \ldots$ run from 0 to 3 and Greek tetrad indices $\alpha, \beta, \ldots$ from 1 to 3. Dropping all non-resonant terms the evolution equations can be found from (3.3) and (3.4).

3.2.2 Comparison with results obtained using QFT methods

The procedure suggested in the previous subsection is here applied to the four-wave interaction case in the center of mass system. The wave vectors of the interacting waves

are denoted by $\mathbf{k}_A$, $\mathbf{k}_B$, $\mathbf{k}_C$, $\mathbf{k}_D$ and polarization states perpendicular to the wave vectors are introduced according to figure 3.1. Using these preliminaries the following set of evolution equations for the field amplitudes can be derived, where the coupling coefficients are functions of the scattering angle θ only.

$$\begin{aligned}\Box E_{A+} &= F_1 E^*_{B+} E_{C+} E_{D+} + F_2 E^*_{B+} E_{C\times} E_{D\times} \\ &\quad + F_3 E^*_{B\times} E_{C\times} E_{D+} + F_4 E^*_{B\times} E_{C+} E_{D\times}\,, \end{aligned} \tag{3.5}$$

$$\begin{aligned}\Box E_{B+} &= F_1 E^*_{A+} E_{C+} E_{D+} + F_2 E^*_{A+} E_{C\times} E_{D\times} \\ &\quad + F_3 E^*_{A\times} E_{C+} E_{D\times} + F_4 E^*_{A\times} E_{C\times} E_{D+}\,, \end{aligned} \tag{3.6}$$

$$\begin{aligned}\Box E_{C+} &= F_1 E^*_{D+} E_{A+} E_{B+} + F_2 E^*_{D+} E_{A\times} E_{B\times} \\ &\quad + F_3 E^*_{D\times} E_{A\times} E_{B+} + F_4 E^*_{D\times} E_{A+} E_{B\times}\,, \end{aligned} \tag{3.7}$$

$$\begin{aligned}\Box E_{D+} &= F_1 E^*_{C+} E_{A+} E_{B+} + F_2 E^*_{C+} E_{A\times} E_{B\times} \\ &\quad + F_3 E^*_{C\times} E_{A+} E_{B\times} + F_4 E^*_{C\times} E_{A\times} E_{B+}\,, \end{aligned} \tag{3.8}$$

where $\Box = \partial^2/\partial t^2 - \partial^2/\partial x^2 - \partial^2/\partial z^2$ and

$$\begin{aligned} F_1 &= \frac{\kappa\left(3+\cos^2\theta\right)^2}{1-\cos^2\theta}\,, \\ F_2 &= -\kappa\left(7+\cos^2\theta\right)\,, \\ F_3 &= \frac{4\kappa\left(2+\cos^2\theta+\cos\theta\right)}{1+\cos\theta}\,, \\ F_4 &= \frac{4\kappa\left(2+\cos^2\theta-\cos\theta\right)}{1-\cos\theta}\,. \end{aligned}$$

The symmetry properties imply that $\Box E_{A\times}$, $\Box E_{B\times}$, $\Box E_{C\times}$ and $\Box E_{D\times}$ can be found from (3.5)–(3.8) respectively simply by interchanging $+$ and $\times$. Note the difference in the behavior of the coupling coefficients in the limit of small scattering angles. This is related to the fact that F_2 and F_3, unlike F_1 and F_4, correspond to a change in the polarization state in addition to scattering an angle θ. As a consistency check, the system can be verified to be energy conserving in the case of long pulses. From the evolution equations it is possible to find the unpolarized differential cross-section [8] as

$$\frac{\partial\sigma}{\partial\Omega} = \frac{|\mathcal{M}|^2}{128\omega^2(2\pi)^2}\,, \tag{3.9}$$

where the square of the scattering matrix amplitude averaged over all polarization states is given by

$$|\mathcal{M}|^2 = \frac{\omega^4\kappa^2}{\sin^4\theta}(\cos^8\theta + 28\cos^6\theta + 70\cos^4\theta + 28\cos^2\theta + 129)\,.$$

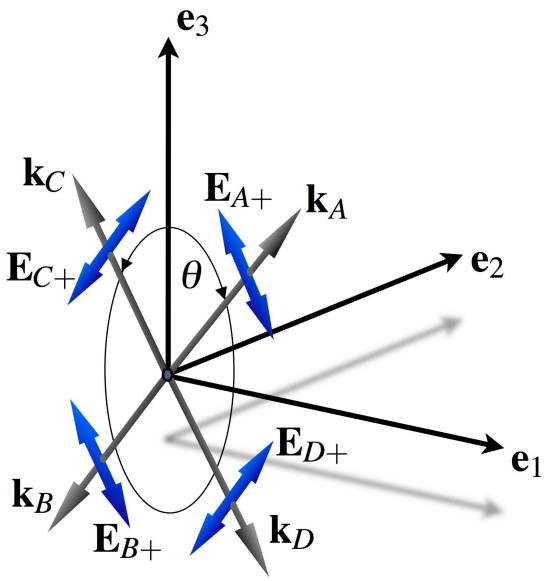

Figure 3.1: Polarization states perpendicular to the wave vectors. The $E_\times$ polarizations coincide with the direction of $\mathbf{e}_2$.

(Equation (3.9) is given in units where $\hbar = c = 1$.) For small scattering angles the result coincides with the cross-section (2.2) for graviton mediated photon-photon scattering obtained using QFT methods discussed in section 2.3.2, but for larger angles the consistency is not flawless as figure 3.2 shows. A possible explanation of the apparent discrepancy can be given by the fact that in [7] the matrix scattering amplitude was used to determine the interaction potential. However, according to [18] such a procedure is not sufficient to fully reproduce the general relativistic potential. It is unclear at this point whether it is possible to improve the QFT calculation to attain perfect agreement with general relativity.

3.3 Wave guides and cavities

In confined spaces the boundary conditions at the surfaces of the walls will impose restrictions on the fields and thereby reduce the number of modes which can propagate inside it to a discrete number. For perfectly conducting walls these boundary conditions simplify to the tangential component, E_t, of the electric field being zero and that the normal component, B_n, of the magnetic field vanishes. These conditions follow from the fact that the electric field inside a perfect conductor is zero together with the continuity of E_t and from the magnetic field being divergence free, respectively. A wave guide can be

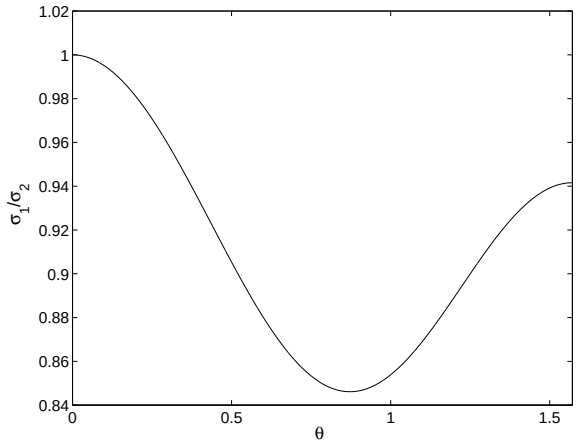

Figure 3.2: The ratio between the cross-section σ_1 obtained with classical general relativity and σ_2 obtained with QFT methods as a function of the scattering angle θ.

described as an infinitely long tube with open ends, where the shape of the cross-section is somewhat arbitrary as long as it is closed. Cutting off a finite part of a wave guide and replacing its open ends with walls gives a cavity, in which the fields will take the form of standing waves. Cavities have proven to be a very useful tool for studying wave interaction phenomena and some of the associated advantages are listed below.

1. The interaction is resonant in a large volume.

2. The growth of the excited mode will not be saturated by convection out of the interaction region.

3. The techniques for detecting weak signals in cavities are well developed [19, 20].

4. It gives a non-zero coupling between parallel plane waves, which is not the case in an unbounded medium.

Assume that we have two pump modes in the cavity exciting a third eigen-frequency through resonant interaction. At some point the dissipation will grow large enough to exactly balance the amplitude growth due to the coupling. To find this saturated amplitude of the excited mode the following procedure is used.

1. Find the linear eigenmodes of the cavity. To minimize the losses due to dissipation we use a cavity with superconducting walls. Even though the conductivity is finite we use boundary conditions for infinitely conducting walls at this stage. Later on the dissipation will be added as a phenomenological term.

2. Choose the frequency matching conditions giving restrictions on the dimensions of the cavity.

3. Perform the variation of the field amplitudes to obtain the evolution equations for the fields.

4. Add dissipation by substituting $d/dt \rightarrow d/dt - K_D$, where K_D depends on the frequency and the quality factor of the cavity. The quality factor is more or less a material characteristic quantity related to the conductivity.

3.3.1 Experimental considerations

When performing experiments on wave interaction in cavities it is of course preferable to maximize the amplitude of the excited wave. However, there are two important limitations to take into consideration. First of all the superconductivity will break down if the amplitude of the magnetic field at the surface rises above the critical value. The critical field depends on the material of the cavity and for a niobium cavity it is approximately 0.28T. Moreover, when the electric field at the surface gets too strong, field emission will take place. This means that electrons will be torn off the walls of the cavity ruining the vacuum inside it. For certain geometries a wise choice of pump modes can be used to circumvent this second limitation.

Using this kind of experimental setup it is apparent that the weak excited mode has to be measured in the presence of the much stronger pump modes. This is difficult even with the best equipment available today. In paper I we suggest a slight modification of the geometry to filter out the excited signal without affecting the interaction considerably. This is done by adding a filtering region, into which only the excited mode can propagate. An example of such a filtering geometry for a cylindrical cavity is shown in figure 3.3. Finite element calculations show that an effective damping of several orders of magnitude can be achieved using this method with a filtering region of roughly the same size as the interaction region, see figure 3.4. The damping is of course strongly dependent on the length of the filtering region. Crudely estimated, the filtering geometry will reduce the number of excited photons per unit volume by a factor 2. Furthermore, some experimental fine-tuning of the eigenfrequencies will be necessary due to the deviation from the cylindrical shape.

3.4 Experimental setup for detection of photon-photon scattering using cavities

As we have seen, studying wave coupling phenomena in cavities has many advantages. We can utilize coherent resonant interaction in a large volume and the techniques for detecting

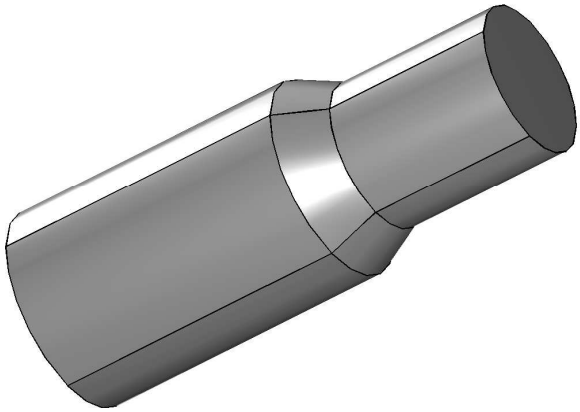

Figure 3.3: Filtering geometry for a cylindrical cavity. Only the excited mode can propagate into the filtering region to the right in the figure.

weak signals in cavities are well developed. Deriving the evolution equations for three-wave interaction in vacuum due to nonlinearities associated with photon-photon scattering leads to the conclusion that a cylindrical geometry is superior to a rectangular prism. This is partly because the coupling per unit volume is slightly higher, but also due to the fact that a wise choice of pump modes eliminates the possibility of field emission. This is achieved by working with transverse electric (TE) modes with no angular dependence, for which the electric field at the boundary vanishes everywhere. For three-wave interaction subjected to the frequency matching condition

$$\omega_3 = 2\omega_1 - \omega_2,$$

the saturated level of the excited mode (denoted by subscript 3) is found to be

$$N_{QED} \propto a^2 z_0 Q^2 \omega_3^5 \left|A_1\right|^4 \left|A_2\right|^2,$$

where a and z_0 is the radius and length of the cavity, Q the quality factor, ω_3 the frequency of the excited wave, A_1 and A_2 the vector potential amplitudes of the pump modes. Notice the strong dependence on the pump amplitudes and the quality factor. Using present day high performance parameter values for superconducting niobium cavities we arrive at 18 excited photons for a specific choice of mode numbers and a cavity volume of approximately $0.5m^3$. This is well above the thermal noise level, which is given by

$$N_{th} = e^{-(\hbar\omega_3/k_B T)},$$

where k_B is Boltzmann's constant and T is the temperature. Thus the phenomenon of photon-photon scattering should be detectable using the suggested technique, even though the required size of the cavity and strengths of the pump modes in practice give a high experimental threshold.

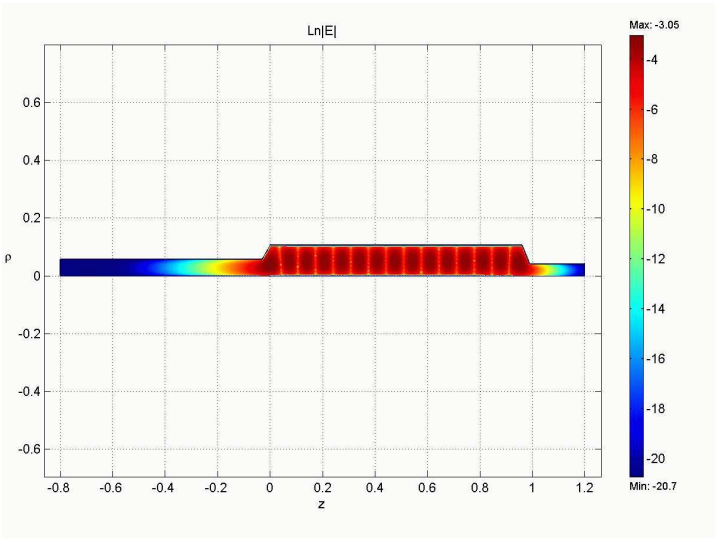

Figure 3.4: Logarithmic plot of the magnitude of the electric field for a TE mode not being able to propagate into the filtering region to the left in the figure. Because of the cylindrical symmetry only one half of the cross-section of the cavity is shown. The small extension to the right is included for generation of pump modes.

The room for improvement of the parameter values really lies in the material of the cavity walls, which determines the quality factor as well as the upper bound for the field strengths.

Chapter 4

Construction of geometries in terms of invariant objects

This chapter starts with a short review of the equivalence problem, i.e. the problem to determine if two geometries are equivalent despite appearing different due to choice of coordinates. We continue with a description of how the procedure of solving this problem can be reversed and turned into a method for constructing new geometries.

4.1 The Equivalence Problem

A geometry can appear quite differently depending on the choice of coordinate system. Given two different metrics, $g_{\mu\nu}(x^\sigma)$ and $\tilde{g}_{\mu\nu}(\tilde{x}^\sigma)$, it is far from trivial to tell by inspection whether they describe the same geometry or not. Even the simplest geometry, such as the Schwarzschild metric describing the gravitational field outside a spherically symmetric object, can look horrible with an inappropriate choice of coordinates. The problem can be summarized as follows. Does there exist a coordinate transformation $\tilde{x}^\mu = \tilde{x}^\mu(x^\nu)$ such that

$$g_{\mu\nu}(x^\sigma) = \frac{\partial \tilde{x}^\alpha}{\partial x^\mu}\frac{\partial \tilde{x}^\beta}{\partial x^\nu}\tilde{g}_{\alpha\beta}(\tilde{x}^\tau) \quad ?$$

It was shown by Cartan [21] that a spacetime is locally completely determined by a set R^{p+1} consisting of the Riemann tensor and a finite number of its covariant derivatives in a frame with constant metric η_{ij}

$$R^{p+1} = \left\{R_{ijkl}, R_{ijkl;m_1}, ..., R_{ijkl;m_1...m_{p+1}}\right\},$$

where p is the smallest integer such that the elements in R^{p+1} are functionally dependent of those in R^p. The components in R^{p+1} should be seen as functions on the ten dimensional frame bundle $F(M)$, i.e. they are functions of both the coordinates x^α and the parameters

ξ^A describing the orientation of the frame. In a 4-dimensional spacetime ξ^A are the parameters of the Lorentz group. By checking the compatibility of the sets R^{p+1} for two geometries it is possible to determine if they only differ in choice of coordinates.

Note that equivalence in local geometry not necessarily means that the global geometry is equivalent. Both the surface of a cone and a plane appear to be flat locally, but are clearly different from a global point of view.

For a more extensive review of the equivalence problem, see [22].

4.1.1 Karlhede classification

The following procedure for checking the equivalence of metrics in practice was developed by Karlhede [22]. As an example we consider the classification of the simple two dimensional metric

$$ds^2 = d\theta^2 + \theta^6 d\varphi^2$$

along with each step.

1. Choose a constant metric.

   Ex. $\eta_{ij} = \begin{bmatrix} 1 & 0 \\ 0 & 1 \end{bmatrix}$

2. Choose an arbitrary fixed tetrad consistent with the previous step and compute the components of the Riemann tensor.
   Ex. $\omega^1 = d\theta,\ \omega^2 = \theta^3 d\varphi \quad \Rightarrow \quad R_{1212} = \frac{R}{2} = -\frac{6}{\theta^2}$

3. Determine the number n_0 of functionally independent components in the set $\{R_{ijkl}\}$.
   Ex. $n_0 = 1$

4. Determine the isotropy group H_0 leaving $\{R_{ijkl}\}$ invariant.
   Ex. $H_0 = O_2$ (rotational group in two dimensions)

5. Choose a standard tetrad in order for the components R_{ijkl} to become as simple as possible and to minimize the functional dependence.
   Ex. The tetrad chosen in step 2 is suitable in this case.

6. Calculate R^1 in the standard tetrad.
   Ex. $R_{;1} = \frac{24}{\theta^3}$

7. Determine the number n_1 of functionally dependent components in R^1.
   Ex. $n_1 = 1$

8. Determine the isotropy group $H_1 \subset H_0$ leaving R^1 invariant.
   Ex. $H_1 = \emptyset$

If $n_1 = n_0$ and $H_1 = H_0$ then R^1 gives a complete local description of the geometry. Otherwise the procedure must be extended to higher covariant derivatives until a set R^m is found for which $n_m = n_{m-1}$ and $H_m = H_{m-1}$. For the considered example $n_2 = n_1 = 1$ and $H_2 = H_1 = \emptyset$.

4.2 Construction of Geometries

This section contains a short motivation of why a method for construction of geometries based on knowledge about the equivalence problem would be useful. Then the procedure of finding the 1-forms and the metric is described in a more detailed mathematical framework. Further information concerning the method can be found in [23].

4.2.1 Motivation

In a comoving tetrad the four-velocity of matter, $u^i = (u^0, 0, 0, 0)$, can be rewritten in terms of some kinematic quantities as

$$u_{i;j} = \sigma_{ij} + \omega_{ij} - \frac{1}{3}h_{ij}\theta + a_i u_j \,, \tag{4.1}$$

where $h_{ij} = g_{ij} - u_i u_j$ is the projection operator onto the space perpendicular to the four-velocity, $\sigma_{ij} = h_i^k h_j^l \left(u_{(k;l)} + \frac{1}{3}\theta h_{kl}\right)$ the shear, $\theta = u^i_{;i}$ the expansion, $\omega_{ij} = h_i^k h_j^l u_{[k;l]}$ the vorticity and $a_i = u_{i;j}u^j$ the acceleration. Moreover, the elements in R^{p+1} can be expressed using the derivatives with respect to the frame vectors, $x^\mu_{|i} \equiv X_i^\nu \frac{\partial x^\mu}{\partial x^\nu}$, and the Ricci rotation coefficients, γ^i_{jk}, some of which can be written as functions of the kinematic quantities defined in (4.1). This indicates that the elements in R^{p+1} correspond to physically measurable quantities. A more formal argument for this can be found by looking at the equation for geodesic deviation. Consider two closely located geodesics, x^μ and y^μ, both parametrized by u. Let η^μ be a vector joining points on the two geodesics with the same parameter value, see figure 4.1. Then it can be shown that the following equation is satisfied in a coordinate basis [24]

$$\frac{D^2\eta^\mu}{du^2} + R^\mu_{\nu\tau\sigma}\eta^\tau \frac{dx^\nu}{du}\frac{dx^\sigma}{du} = 0 \,. \tag{4.2}$$

Here D/du is the absolute derivative along the curve. It is obvious from (4.2) that the dynamical behaviour of the system is closely related to the components of the Riemann tensor. This suggests that it might be a good idea to try reversing the scheme used in the equivalence problem. Thus we start out by specifying the components in R^{p+1} and impose certain conditions for the set to describe a geometry. In this way it is easy to impose physical requirements on the wanted space-time and moreover the method has the advantage of being coordinate invariant.

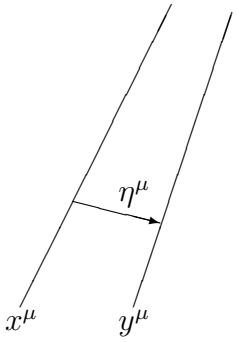

Figure 4.1: The two geodesics x^μ and y^μ are separated by η^μ.

4.2.2 Integrability conditions

A random choice of elements in R^{p+1} will of course probably not correspond to something physically acceptable or even a geometry. The natural question is therefore which conditions R^{p+1} must satisfy in order to describe a geometry. The problem can be reformulated equivalently as follows.

When does there exist ten linearly independent 1-forms, $\{\omega^i, \omega^i_j\}$, satisfying Cartan's equations

$$\begin{aligned} d\omega^i &= \omega^j \wedge \omega^i_j \,, \\ d\omega^i_j &= -\omega^i_k \wedge \omega^k_j + \frac{1}{2} R^i_{jkl} \omega^k \wedge \omega^l \,, \end{aligned} \tag{4.3}$$

where $\omega^i_j = \gamma^i_{jk}\omega^k + \tau^i_j$ and τ^i_j are the generators of the generalized orthogonal group, reproducing R^{p+1} through

$$\begin{aligned} dR_{ijkl} &= R_{mjkl}\omega^m_i + R_{imkl}\omega^m_j + R_{ijml}\omega^m_k + R_{ijkm}\omega^m_l + R_{ijkl;m}\omega^m \\ &\vdots \\ dR_{ijkl;m_1\ldots m_p} &= R_{mjkl;m_1\ldots m_p}\omega^m_i + \ldots + R_{ijkl;m_1\ldots m_{p-1}m}\omega^m_{m_p} \\ &\quad + R_{ijkl;m_1\ldots m_{p+1}}\omega^{m_{p+1}} \quad ? \end{aligned} \tag{4.4}$$

The first of Cartan's equations (4.3) tells us how the 1-forms and the connection 1-forms, ω^i_j, are related while the second gives the connection between the 1-forms and the Riemann tensor. If we denote the set $\{\omega^i, \omega^i_j\}$ by $\{\omega^I\}$, where $I = 1, \ldots, n(n+1)/2$ and n is the

dimension of the manifold, Cartan's equations can be written more compactly as

$$d\omega^I = \frac{1}{2} C^I_{JK} \omega^J \wedge \omega^K \,.$$

Consequently the C^I_{JK} essentially contain the same information as the Riemann tensor. Taking the exterior derivative $dC^I_{JK} = C^I_{JK|L}\omega^M$ and comparing with (4.4) we find that the information in the first covariant derivatives of the Riemann tensor is contained in $C^I_{JK|L}$. Thus we can use the set

$$C^p = \left\{ C^I_{JK}, C^I_{JK|L}, \ldots, C^I_{JK|L_1 \ldots L_p} \right\}$$

instead of R^p. Assume that we have k functionally independent quantities, I^α, in C^p and consider the exterior derivative

$$dI^\alpha = I^\alpha_{|M} \omega^M \,.$$

In the case of no symmetries we can solve for the 1-forms as

$$\omega^M = I^M_\alpha dI^\alpha \,,$$

where $I^\alpha_{|M} I^M_\beta = \delta^\alpha_\beta$. It is just a matter of finding the inverse of the matrix $I^\alpha_{|M}$, which is a subset of C^{p+1}. We conclude that C^{p+1}, or equivalently R^{p+1}, completely determines the geometry. If there are symmetries, the number of functionally independent quantities, k, in C^p will be less than $n(n+1)/2$, but C^{p+1} still determines the geometry locally. Now we can only solve for part of the 1-forms as

$$\omega^A = I^A_\alpha \left(dI^\alpha - I^\alpha_{|P} \omega^P \right) \,,$$

where $A = 1, 2, \ldots, k$ and $P = k+1, k+2, \ldots, n(n+1)/2$. Moreover, it can be shown that the first k of Cartan's equations are equivalent to

$$d^2 I^\alpha \equiv d\left(I^\alpha_{|K} \omega^K \right) = 0 \,.$$

Thus, if we have symmetries, some additional condition is needed to ensure that all Cartan's equations are satisfied. The necessary condition is that

$$d^2 \omega^P \equiv d\left(\frac{1}{2} C^P_{JK} \omega^J \wedge \omega^K \right) = 0 \,.$$

The results can be summarized in the following theorem.

Theorem A

R^{p+1} describes a geometry if and only if

- C^I_{JK} have Riemannian form
- $C^I_{JK|L} = C^I_{JK,\alpha} I^\alpha_{|L}$ etc.
- $d^2 I^\alpha = 0$
- $d^2 \omega^P = 0$

The integrability conditions are equivalent to the Ricci identities plus some of the Bianchi identities.

In practice it is more convenient to work in a fixed frame instead of keeping the explicit dependence on the parameters of the Lorentz group, giving the following set of equations

$$x^\alpha_{[|i,\beta} x^\beta_{|j]} + x^\alpha_{|m} \gamma^m_{[ij]} = 0\,,$$
$$R^a_{bij} = 2\gamma^a_{b[j,\alpha} x^\alpha_{|i]} + 2\gamma^{ak}_{[j} \gamma_{bki]} + 2\gamma^a_{bk} \gamma^k_{[ij]}\,,$$

where R^{p+1} only depends on the essential coordinates, x^α, and rotations in the ab-planes due to the symmetries.

4.2.3 Finding the metric

In order to understand this part it is essential to have some understanding of symmetry groups and therefore we start out with a short review of some basic concepts.

Symmetry Groups

Invariance is a key concept when it comes to understanding physical phenomena. It is closely related to the occurence of conservation laws for physical quantities. For example conservation of angular momentum is a consequence of rotational invariance. The connection between invariance under a group of transformations and conserved quantities is described by Noether's theorem.

A group with manifold structure is called a Lie group and furthermore a group of transformations which leaves the metric invariant is called an isometry group. The generators ξ_μ of an isometry group, the Killing vectors, can be interpreted as vectors pointing in the directions where the metric is unchanged in the case of translational symmetry. On the other hand, a linear combination of the Killing vectors that is zero at some point generates a rotational symmetry of the metric at that point. By definition

$$\mathcal{L}_\xi g = 0\,,$$

where $\mathcal{L}_\xi$ is the Lie-derivative in the direction of ξ. The Killing vectors satisfy some commutation relations called a Lie-algebra according to

$$[\xi_I, \xi_J] = \tilde{C}_{IJ}^K \xi_K \,,$$

where $\tilde{C}_{IJ}^K$ are called structure constants. Symmetry groups are divided into two categories depending on the dimension of the corresponding orbits, which are defined as submanifolds determined by the group action. If a group has the same dimension as its orbits, it is acting simply transitive and otherwise multiply transitive. Groups acting simplify transitive have the useful property that it is always possible to find an invariant basis, $\{X_I\}$, for which

$$\mathcal{L}_{\xi_I} X_J = 0 \,.$$

In such a basis the 1-forms satisfy the relation

$$d\omega^I = \frac{1}{2} \tilde{C}_{JK}^I \omega^J \wedge \omega^K \tag{4.5}$$

and the equivalent commutator relation among the basis vectors is given by

$$[X_I, X_J] = -\tilde{C}_{IJ}^K X_K \,.$$

Method for finding the full metric

In section 4.2.2 we concluded that we can not solve for all of the 1-forms if there are symmetries. However, the property (4.5) of an invariant basis mentioned in the previous section enables us to extract information about the 1-forms we could not find due to symmetries. Projecting Cartan's equations onto the orbits and comparing with tables over known isometry algebras, we can make an ansatz for the remaining 1-forms giving a set of differential equations, which are often integrable. If the ansatz reproduces the initial set R^{p+1}, we have found the full metric and otherwise we have to modify the ansatz and repeat the procedure. The main reason for working on the frame bundle is that the isometry group always acts simplify transitive on $F(M)$.

Chapter 5

Cosmology

Cosmology is a branch of astronomy which deals with large scale phenomena such as the structure and evolution of the universe. This chapter is intended to give a brief introduction to spatially homogeneous perfect fluid models in cosmology.

5.1 Perfect fluid models

At large length scales it is reasonable to depict the universe as a continuous fluid. A perfect fluid is defined as a fluid or gas without anisotropic pressure, viscosity or heat flow. If the mean free path between particle collisions is much less than the scales of physical interest, the fluid can be considered as perfect. Based on observations of the universe, the perfect fluid assumption seems justifiable. The energy-momentum tensor for a perfect fluid is given by

$$T_{ij} = (\rho + p)u_i u_j - p g_{ij} \,,$$

where ρ is the restframe density, p the isotropic pressure and u^i the four-velocity of the fluid. In a comoving frame where $u^i = (1, 0, 0, 0)$ this simplifies to $T_{ij} = diag(\rho, p, p, p)$. The perfect fluid model is often used together with a linear equation of state simply because a more complicated equation of state would shatter all hopes of finding any solutions to Einstein's equations. Moreover, two interesting subcases can be found. When the pressure is zero we have dust, which is a good approximation for any form of non-relativistic fluid or gas. The other interesting case is when $p = \frac{1}{3}\rho$, representing a fluid of ultra-relativistic particles in thermal equilibrium and is referred to as radiation.

5.1.1 Homogeneous, isotropic models - Friedmann models

When the field of cosmology was young and the available observational data was very limited, a widely used assumption when modelling the universe was the cosmological

principle. It says that the universe is both homogeneous and isotropic on sufficiently large scales. Recent observations indicate that this is at least approximately true. The most general metric describing a universe satisfying the cosmological principle is the Robertson-Walker (RW) metric. Using comoving coordinates, $x^\mu = (\tau, r, \theta, \varphi)$, it is given by

$$ds^2 = (c\tau)^2 - a(\tau)^2 \left[\frac{d\tau^2}{1 - Kr^2} + r^2 \left(d\theta^2 + \sin^2 \theta d\varphi^2 \right) \right] ,$$

where τ is the proper time and $a(\tau)$ is the scale factor. K is a curvature parameter which can be scaled to take only the values -1, 0 and 1 which can be interpreted as an open, flat and closed universe respectively. The field equations for a metric of RW type, the Friedmann equations, are

$$\ddot{a} = -\frac{4\pi}{3} G \left(\rho + 3\frac{p}{c^2} \right) a \,, \tag{5.1}$$

$$a\ddot{a} + 2\dot{a}^2 + 2Kc^2 = 4\pi G \left(\rho - \frac{\pi}{c^2} \right) a^2 \,. \tag{5.2}$$

Cosmological models corresponding to solutions of (5.1) and (5.2) are called Friedmann-Roberson-Walker (FRW) models. For a flat universe in the cases of dust and radiation the Friedmann equations can be directly integrated. In 1967 Sachs and Wolfe used a Fourier transformation method to find a class of solutions to the linear perturbation problem around a flat FRW universe [25]. Four years later White showed by direct integration that a restriction used by Sachs and Wolfe was unnecessary and that the solution they found actually was the most general C^∞ solution [26].

5.1.2 Homogeneous, anisotropic models - Bianchi types

Consider the class of cosmological models which are spatially homogeneous, but anisotropic. Depending on the possible symmetries within this class it can be divided further into nine subclasses called Bianchi types I-IX. This can be expressed in terms of the structure constants in the following way. The structure constants can be decomposed into a symmetric 3×3 matrix $N^{\alpha\beta}$ and a three-vector A^α according to the Ellis-MacCallum scheme [27] as

$$\frac{1}{2} C^\alpha_{\beta\delta} \epsilon^{\beta\delta\gamma} = N^{\alpha\gamma} + \epsilon^{\alpha\gamma\beta} A_\beta \,,$$

which implies

$$N^{\alpha\delta} = \frac{1}{2} \left[C^\alpha_{\beta\gamma} \epsilon^{\beta\gamma\delta} - C^\gamma_{\beta\gamma} \epsilon^{\beta\alpha\delta} \right] .$$

Now the conditions for the different Bianchi types can be expressed in a simple way in terms of $N^{\alpha\beta}$ and A^α, which is summarized in table 5.1. Note that there is one class of homogeneous, anisotropic solutions that does not fit into the Bianchi scheme called the Kantowski-Sachs solutions.

Bianchi type		
I	$\mathbf{N} = 0$	$A_i = 0$
II	$\mathbf{N} = diag(1,0,0)$	$A_i = 0$
III	$\mathbf{N} = -\frac{1}{2}\alpha$	$A_i = -\frac{1}{2}\delta_3^i$
IV	$\mathbf{N} = diag(1,0,0)$	$A_i = -\delta_3^i$
V	$\mathbf{N} = 0$	$A_i = -\delta_3^i$
VI_{-1}	$\mathbf{N} = -\alpha$	$A_i = 0$
$\mathrm{VI}_{h\neq -1}$	$\mathbf{N} = \frac{1}{2}(h-1)\alpha$	$A_i = -\frac{1}{2}(h+1)\delta_3^i$
VII_0	$\mathbf{N} = diag(-1,-1,0)$	$A_i = 0$
$\mathrm{VII}_{h\neq 0}$	$\mathbf{N} = diag(-1,-1,0) + \frac{h}{2}\alpha$	$A_i = -\frac{h}{2}\delta_3^i$
VIII	$\mathbf{N} = diag(-1,1,1)$	$A_i = 0$
IX	$\mathbf{N} = \delta_{ij}$	$A_i = 0$

Table 5.1: Summary of the Bianchi classification.

where

$$\alpha = \begin{bmatrix} 0 & 1 & 0 \\ 1 & 0 & 0 \\ 0 & 0 & 0 \end{bmatrix} .$$

5.2 Cosmological constant - Dark energy

5.2.1 Motivation

The cosmological constant was introduced by Einstein in the days when the general opinion was that the universe is static. From the Friedmann equations it is clear that either the pressure or the energy density must be negative to get a static universe in the absence of a cosmological constant. The field equations are modified, without destroying the covariance, in the following way

$$R_{ij} - \frac{1}{2}Rg_{ij} = T_{ij} + \Lambda g_{ij} \,,$$

where Λ is the cosmological constant. This is equivalent to introducing an effective pressure $\tilde{p}$ and energy density $\tilde{\rho}$ as

$$\tilde{p} = p - \Lambda \,, \;\; \tilde{\rho} = \rho + \Lambda \,.$$

However, as we will see below, observations contradict the assumption of the universe being static and it is now considered likely that the universe is expanding at an accelerated rate, even though a certain degree of uncertainty remains in this issue. Generally, a

positive cosmological constant has an accelerating effect and thus the idea is kept, despite the reason for its origin.

Alternative explanations of the observed expansion rate can be found by introducing a slowly varying scalar field called quintessence or by using inhomogeneous models, see e.g. [28] and [29] respectively.

5.2.2 Observational data

The expansion of the universe can be measured indirectly by looking at the redshift of type Ia supernovae. These objects are suitable for the purpose since they have a well-defined brightness, which is a necessary property in order to relate redshift and distance via Hubble's law. Recent data, e.g. from the *High-z Supernova Search Team* [30] and the *Supernova Cosmology Project* [31], support the idea of the universe being expanding at an accelerated rate. Moreover, measurements of the cosmic microwave background (CMB) indicate that the total amount of matter (including non-baryonic) in the universe estimated by the dynamics of galaxy clusters is just a fraction of what is needed to attain consistency with the measured geometry. Consequently, this suggests the existence of some additional form of energy, called dark energy. The distribution of mass-energy according to recent meaurements, e.g. by the *Wilkinson Microwave Anisotropy Probe* (WMAP) [32], is shown in figure 5.1. The nature of the dark energy is to a large extent

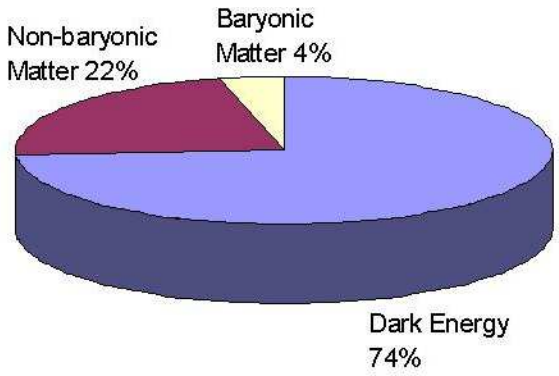

Figure 5.1: Distribution of mass-energy in the universe. The non-baryonic matter is also referred to as dark matter.

unknown, despite its relative abundance. However, the distribution appears to be very homogeneous in space and time-independent [32, 33], making the cosmological constant a suitable model. In paper II linear perturbations around a flat FRW universe with a cosmological constant are studied.

Dark matter is an alternative term for non-baryonic matter originating from the interaction properties being only gravitational, i.e. not visible in the usual sense that it interacts with or emits electromagnetic radiation. At this point there are several kinds of

particles being possible dark matter candidates. The interaction properties constitute a high threshold for experiments with the purpose of gaining further knowledge about this dark matter.

5.3 The Sachs-Wolfe effect

Photons propagating in space, which encounter metric perturbations, will experience a frequency shift. For simplicity let us consider a metric perturbation in the form of a potential well. A photon entering the well will gain energy and thus be blueshifted while a photon leaving the well will experience a loss of energy, i.e. a redshift. If we assume that the depth of the well is constant throughout the whole passage, the blueshift and the redshift will exactly cancel each other. However, if the well gets shallower or deeper during the passage, the photon will be subject to a net frequency shift. Moreover, a second contribution to the effect comes from the fact that a change of the depth of the well is associated with a stretching of the fabric of spacetime itself. The situation is shown in figure 5.2. Consequently this will create a temperature anisotropy in the CMB. This effect is known as the Sachs-Wolfe effect and it is expected to be the dominante contribution on large scales. The relative temperature variation can be computed [25] as

$$\frac{\delta T}{T} = \frac{1}{2}\int_0^{\eta_R-\eta_E} \left(\frac{\partial h_{\alpha\beta}}{\partial \eta} e^\alpha e^\beta - 2\frac{\partial h_{0\alpha}}{\partial \eta} e^\alpha \right) dw \,, \tag{5.3}$$

where $h_{\alpha\beta}$ is the metric perturbation, η the conformal time, η_R and η_E the time of reception and emission, w the affine length along the null geodesic of propagation and e^α the tangent three-vector of the photon path normalized as $e^\alpha e_\alpha = -1$.

5.4 Perturbations of FRW models with a cosmological constant

In paper II we perform an analytic integration of the perturbed field equations around a flat FRW universe with a cosmological constant for the case of no pressure. The technique is an adjusted version of the one used by White in the case without a cosmological constant [26]. It turns out that the key step in the integration procedure is introducing a comoving time t. The complete solution for the metric perturbation, $h_{\alpha\beta}$, is lengthy so only the density perturbation is given here as

$$\delta\rho = \frac{C_M}{2a_0^3}\frac{\cosh(Ct)}{\sinh^3(Ct)}\left(\nabla^2 A - \frac{3\nabla^2 B}{2^{4/3}a_0^2 C^2} I\right) , \tag{5.4}$$

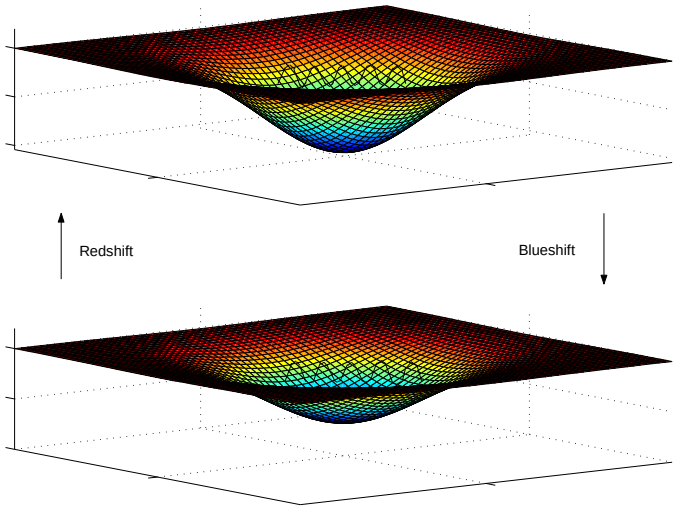

Figure 5.2: The stretching of the fabric of spacetime will cause a frequency shift for a photon passing through.

where C_M and a_0 are constants, A is an arbitrary spatial function, B and C are spatial functions related to $h_{\alpha\beta}$ as

$$\begin{aligned} h^{0\alpha} &= \frac{1}{a}\nabla^2 C^\alpha \,, \\ \nabla^2 B &= \frac{1}{2}S^{\mu\nu}_{,\mu\nu} + \frac{1}{3}\nabla^2 h \,, \end{aligned}$$

where $S_{\mu\nu}$ is the trace-free part of $h_{\alpha\beta}$ and I is the elliptic integral

$$I = 2^{-2/3}\sqrt{3\Lambda}\int_0^t \frac{\sinh^{2/3}(C\tau)}{\cosh^2(C\tau)d\tau}\,.$$

The time dependence of the two contributions to the density contrast is plotted in figure 5.3, making it clear that one is relatively increasing and the other relatively decreasing, both approaching asymptotic values. Calculating the Sachs-Wolfe temperature variations in the CMBR associated with the obtained metric perturbations according to (5.3), we conclude that the presence of a cosmological constant gives rise to an overall attenuation factor of 3 for the power spectrum. Our results are consistent with Sachs and Wolfe in the limit of a vanishing cosmological constant.

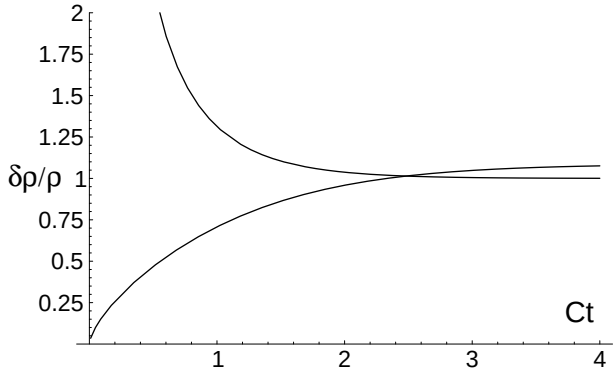

Figure 5.3: The two contributions to the density contrast. The relatively decreasing curve corresponds to the first term in (5.4).

5.5 Rotating models

A homogeneous cosmological model, for which the fluid velocity vector is orthogonal to the hypersurfaces of homogeneity, is called orthogonal. If this condition is not met the term tilted is used. A Bianchi cosmology must be tilted in order to have non-vanishing vorticity.

Vorticity is a local property of spacetime and should not be thought of as a situation where the entire universe is rotating around a fixed point, but rather like matter is rotating around the non-rotating observer at each point. Consequently, a rotating model will not look spatially homogeneous to an observer comoving with the fluid.

An interesting property of rotating cosmologies is that they allow for the existence of closed timelike curves, a phenomenon occuring in e.g. the Gödel universe [34]. If two events are joined by a timelike curve, it means that it is possible for a particle to visit both events. Thus closed timelike curves would in principle enable time travelling. This will of course mean a violation of causality and is in some sense inconsistent with the free will, but we will not take the philosophical discussion further here. The point is that this is an undesirable property for a realistic cosmological model. Note however that a non-vanishing vorticity does not necessarily imply the existence of closed timelike curves. Is there then any further features concerning the vorticity associated with a realistic cosmological model? Based on observations, a realistic model of the universe requires that the vorticity and other perturbations are small compared to the expansion, essentially meaning that it is reasonably close to the Big Bang model. However, it is a shortcoming that very few exact solutions belonging to this category are known. There is actually only one known exact homogeneous perfect fluid solution with both vorticity and expansion, which was found by Rosquist [35] and belongs to Bianchi type VI_0.

5.5.1 Observations

The methods for investigating the possibility of rotation in the universe can be divided into two categories. First we have the direct measurement techniques, where the most successful method is based on measuring the orbits of the planets in our solar system relative to the stars in the background. A rotating background would imply a deviation from the predictions by Kepler's laws with general relativistic corrections included. The second category is characterized by the fact that the methods are highly dependent on a certain cosmological model, which makes them somewhat unreliable. Here the idea is to identify a quadrupole moment in the intensity distribution of the CMB, usually by relating observational data to perturbative studies of cosmological models. The two categories have in common that they do not provide proof for a rotating universe, but rather an upper bound for the rotation. Using the direct method suggested above, Clemence calculated this upper bound to be 0.1 arcseconds per century [36]. Surprisingly, to my knowledge there has not been much improvement of this limit during the last 50 years. Here it should be mentioned that the model depending techniques provide upper bounds that are several orders of magnitude smaller, see e.g. [37, 38].

5.5.2 Tilted cosmological models of Bianchi type V

Applying the method described in chapter 4 to find cosmological models of Bianchi type V and I yields a general system of five coupled, first order differential equations. The system is integrable and the full line-element can be found in terms of quadratures if the system of ODEs is solved. The linearized equations around the open Friedmann universe can be completely integrated for the dust and radiation case. Locally rotationally symmetric solutions is a subclass studied in [39] which can be completely integrated in the case of vanishing pressure and cosmological constant. Here two types of solutions are found, one where the hypersurfaces of homogeneity remain spacelike and one for which they change from being spacelike to being timelike. A numerical study of the general system, using the Runge-Kutta method with a fourth order truncation error with respect to the step length, supports both the analytical results in the LRS case as well as the perturbative calculations. The asymptotic behaviour of Bianchi type V models has recently been studied in [40] using dynamical system analysis. It was found that for $2/3 < \gamma < 2$ these models approach the Milne universe, i.e. Minkowski in an expanding coordinate system, in the low density limit. This conclusion is confirmed by the numerical runs. Less is known about the behaviour in the high density limit, but the numerical study indicates that the tilt grows to infinity except for some special initial values.

Chapter 6

Rotating stars in general relativity

An interesting prediction with no Newtonian counterpart, appearing when a rotating object is treated in a general relativistic framework, is the Lense-Thirring effect [41, 42]. The basic idea is that inertial frames are dragged along with the rotation of the object. In April 2007 a satellite called Gravity Probe B [43] was launched for the purpose of measuring this effect using extremely sensitive gyroscopes. The project is at the moment in the data analyzing phase.

Even though relativistic stars can appear to have complicated structures with solid crust, magnetic field etc., it is possible to make accurate predictions about their properties based on some simple assumptions. First of all a perfect fluid description of matter seems reasonable, since observations of pulsar glitches show that the relative deviations from a perfect fluid equilibrium are of order 10^{-5} [44]. More of these assumptions will be discussed in section 6.1 in connection with the Hartle formalism for slow rotation. There are several other schemes, apart from the Hartle formalism, available for studying rotating relativistic stars such as the Newton-Raphson linearization scheme by Butterworth and Ipser [45], the scheme by Komatsu *et al.* using Green´s functions [46, 47], the minimal surface scheme due to Neugebauer and Herold [48] and the spectral schemes by Bonazzola *et al.* [49, 50] and Ansorg *et al.* [51]. However, we will focus solely on the Hartle formalism in this chapter, since it is the foundation for the included papers on this topic. For a more extensive review of the field, see [52].

6.1 The Hartle formalism

In 1967 a perturbative scheme for studying equilibrium configurations of rotating stars was developed by Hartle [53]. The most important assumptions for this formalism to be valid are

1. **Barotropic equation of state**:
   The equation of state is independent of the temperature leaving a one parameter

relation betweeen the pressure, p and energy density, ρ,

$$p = p(\rho)\,.$$

This description is valid for cold neutron stars, for which the thermal energy is negligible compared to the Fermi energies of the interior.

2. **Axial and reflection symmetry**:
   Axial symmetry implies that there are no time-dependent moments of the mass distribution and thus no radiation of gravitational waves, which is a necessary condition for the existence of equilibrium configurations.

3. **Uniform rotation**:
   The four-velocity can be written on the form

$$u^\mu = (u^t, 0, 0, \Omega u^t)\,,$$

   implying that the shear vanishes. There are several damping mechanisms for differential rotation for neutron stars suggesting that this is a reasonable assumption. The damping due to kinematical shear viscosity has been investigated in [54, 55, 56], while convective and turbulent motions has been considered in [57]. On shorter timescales the magnetic braking by Alfvén waves has been suggested to be the most important contribution [58].

4. **Slow rotation**:
   Fractional changes in pressure, density and gravitational field due to the rotation should remain small. This condition can be interpreted as a situation where all particles are moving with nonrelativistic velocities.

The metric of a star satisfying the conditions above can up to second order in the rotational parameter, Ω, be written in the form

$$ds^2 = (1+2h)A^2dt^2 - (1+2m)\frac{1}{B^2}dr^2 - (1+2k)r^2\left[d\theta^2 + \sin^2\theta\,(d\varphi - \omega dt)^2\right]. \quad (6.1)$$

Here the frame dragging effect mentioned above appears in the $t\varphi$ cross-term. Due to the symmetries, an expansion of the quantities appearing in the metric in terms of Ω results in A, B being zeroth order, ω first order and h, k, m second order. ω is a function of r only as a consequence of the requirements of regularity at the center and asymptotic flatness. The angular dependence of the second order functions can be found by an ansatz in terms of Legendre polynomials as

$$h = \sum_{i=0}^{\infty} h_i(r)P_i(\cos\theta)\,, \qquad k = \sum_{i=0}^{\infty} k_i(r)P_i(\cos\theta)\,,$$

$$m = \sum_{i=0}^{\infty} m_i(r)P_i(\cos\theta)\,.$$

With this ansatz the equations for h, k and m separate and it turns out that no terms with $i > 2$ are coupled to the rotation. Moreover, the reflection symmetry excludes all odd terms in the ansatz. Thus it is possible to write the second order functions in a simplified form

$$h = h_0 + h_2 P_2(\cos\theta)\,, \qquad m = m_0 + m_2 P_2(\cos\theta)\,,$$
$$k = k_2 P_2(\cos\theta)\,.$$

6.2 Matching of metrics

Consider the problem of matching two N-dimensional metrics at a $(N-1)$-dimensional hypersurface. In the case of rotating stars it is a matter of finding the surface S of the star, which is given by the zero pressure surface, and then matching the metrics of the vacuum and the matter region on S. The theory for the matching was developed by Darmois and Israel [59, 60].

6.2.1 Darmois-Israel procedure

The Darmois-Israel procedure consists of two conditions, the more obvious of which states that the projected metrics of the two regions, A and B, should agree on the matching surface

$$ds^2_{(A)}\big|_S = ds^2_{(B)}\big|_S\,.$$

Moreover the projected second fundamental forms should satisfy

$$K_{(A)}\big|_S = K_{(B)}\big|_S\,, \tag{6.2}$$

where

$$K \equiv K_{ab}dx^a dx^b \equiv h^c_a h^d_b n_{(c;d)} dx^a dx^b$$

and

$$h^b_a = n_a n^b + \delta^b_a$$

is the projection operator onto the tangent plane of the hypersurface. The condition (6.2) essentially guarantees that the normal vectors should diverge smoothly along the matching surface, see figure 6.1. An alternative interpretation is that there are no shells of matter on the matching surface. From a more mathematical point of view, this means that there are no δ-functions appearing in the Ricci tensor.

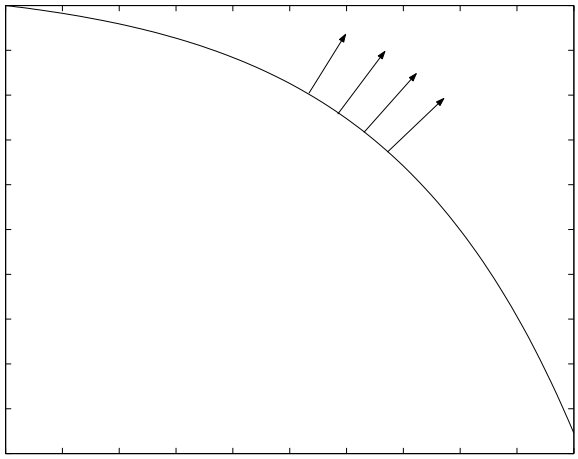

Figure 6.1: The projected second fundamental forms agree on the surface, which implies that the normal vectors diverge smoothly.

6.3 Petrov classification

First of all I want to point out that even though the Petrov classification is mentioned here in the context of rotating massive objects, it can be applied to more general spacetimes as well.

Using spinor formalism, the Riemann tensor can be irreducibly decomposed in a similar way as in the four vector case. The spinor equivalents of the Weyl tensor, the trace-free part of the Ricci tensor and the curvature scalar are Ψ_{ABCD}, $\Phi_{AB\dot{C}\dot{D}}$ and Λ respectively. The symmetric properties of the Weyl spinor imply that it can be written as a symmetrized product of four principal 1-spinors

$$\Psi_{ABCD} = \alpha_{(A}\beta_B\gamma_C\delta_{D)} \,.$$

The classification is based on how many of these principal spinors which are proportional to one another. In table 6.1 the symmetry properties of the Weyl spinor characterizing the six different Petrov types are summarized. Petrov type I represents the lowest degree

Petrov type	
I	$\Psi_{ABCD} = \alpha_{(A}\beta_B\gamma_C\delta_{D)}$
II	$\Psi_{ABCD} = \alpha_{(A}\alpha_B\beta_C\gamma_{D)}$
III	$\Psi_{ABCD} = \alpha_{(A}\alpha_B\alpha_C\beta_{D)}$
D	$\Psi_{ABCD} = \alpha_{(A}\alpha_B\beta_C\beta_{D)}$
N	$\Psi_{ABCD} = \alpha_{(A}\alpha_B\alpha_C\alpha_{D)}$
0	$\Psi_{ABCD} = 0$

Table 6.1: Summary of the Petrov classification. α_A, β_A, γ_A and δ_A are not proportional.

of symmetry and thus spacetimes in this class are called algebraically general, while spacetimes belonging to the five remaining Petrov types are called algebraically special.

A way of determining the Petrov type is to define nonzero spinors η^a satisfying

$$\Psi_{abcd}\eta^a\eta^b\eta^c\eta^d = 0$$

and let

$$x = \frac{\eta^1}{\eta^0}\,.$$

Solving the equation

$$\Psi_0 + 4\Psi_1 x + 6\Psi_2 x^2 + 4\Psi_3 x^3 + \Psi_4 x^4 = 0\,, \tag{6.3}$$

where $\Psi_0 \equiv \Psi_{0000}$, $\Psi_1 \equiv= \Psi_{0001}$, $\Psi_2 \equiv \Psi_{0011}$, $\Psi_3 \equiv \Psi_{0111}$, $\Psi_4 \equiv \Psi_{1111}$ then gives the principal null directions as $\eta^a\bar{\eta}^{\dot{a}}$. Now the multiplicity of the principal null directions determines the Petrov type. It was shown in [61] that these principal null directions actually are directly observable quantities of the spacetime. By looking at the distorsion of a distant sphere in the limit when the distance approaches zero, the principal null directions can be indentified as directions where the distorsion vanishes.

In practice the classification is done by chosing a null tetrad $\{k^\mu, l^\mu, m^\mu, \bar{m}^\mu\}$, computing

$$\begin{aligned}
\Psi_0 &= C_{abcd}k^a m^b k^c m^d\,, \quad & \Psi_3 &= C_{abcd}k^a l^b \bar{m}^c l^d\,,\\
\Psi_1 &= C_{abcd}k^a l^b k^c m^d\,, & \Psi_4 &= C_{abcd}\bar{m}^a l^b \bar{m}^c l^d\,,\\
\Psi_2 &= C_{abcd}k^a m^b \bar{m}^c l^d\,,
\end{aligned}$$

and checking the multiplicity of the roots of (6.3).

6.3.1 Specifying Petrov type instead of Equation of state

The most common approach, when studying perfect fluid models of rotating stars, is to explicitly specify an equation of state as a complement to the field equations. An alternative method is to impose a condition on the Petrov type of the fluid region and thus leave the equation of state undetermined at this point to avoid making the system overdetermined. The choice of a suitable Petrov type can be narrowed down considerably due to the fact that it can be shown that physically realistic prefect fluid models of rotating stars cannot be of Petrov type II, III, N or 0 [62]. Further information concerning the choice of Petrov type can be acquired by considering known exact solutions. The nonrotating spherically symmetric solutions, all being of Petrov type D or 0, can give a hint since they should be possible to obtain in the slow rotation limit. Summing the information together indicates that Petrov type D should be a good choice. An advantage associated with specifying Petrov type instead of equation of state for the present application is that certain scaling invariances will appear in the system.

6.4 Some important exact solutions

This section contains a short description of some exact solutions that are important in the sense that they appear as special cases of the class studied in papers V and VI.

6.4.1 The Wahlquist solution

The Wahlquist solution [63] is an interior, rotating perfect fluid solution of Petrov type D, which is axisymmetric and stationary. Using comoving, pseudo-confocal, spatial coordinates $\{\zeta, \xi, \theta\}$ the line element can be expressed as

$$\begin{aligned} ds^2 = & - \frac{1}{\phi^2}\left(dt - Ad\theta\right)^2 + r_0^2(\zeta^2+\xi^2) \\ & \times \left[\frac{d\zeta^2}{(1-k^2\zeta^2)h_1} + \frac{d\xi^2}{(1+k^2\xi^2)h_1} + \frac{\delta^2 h_1 h_2}{h_1-h_2}d\theta^2\right], \end{aligned}$$

where

$$\frac{1}{\phi^2} = \frac{h_1-h_2}{\zeta^2+\xi^2}, \qquad A = \delta r_0\left[\frac{\xi^2 h_1 + \zeta^2 h_2}{h_1-h_2} - \xi_A^2\right],$$

$$\begin{aligned} h_1(\zeta) &= 1+\zeta^2 - \frac{2m}{r_0}\zeta(1-k^2\zeta^2)^{1/2} + \frac{\zeta}{\kappa^2}\left[\zeta - \frac{1}{k}(1-k^2\zeta^2)^{1/2}\sin^{-1}(k\zeta)\right], \\ h_2(\xi) &= 1-\xi^2 - \frac{2b}{r_0}\xi(1+k^2\xi^2)^{1/2} - \frac{\xi}{\kappa^2}\left[\xi - \frac{1}{k}(1+k^2\xi^2)^{1/2}\sinh^{-1}(k\xi)\right]. \end{aligned}$$

Here k, κ, m, b, r_0, ξ_A and δ are constants, some of which are related to each other. The equation of state is linear and reads

$$\rho + 3p = \frac{k^2}{r_0^2\kappa^2}.$$

For several reasons this metric is not an acceptable model of an isolated rotating object.

1. The shape of the constant pressure surfaces is prolate, i.e. the radius is extended at the poles and shortened at the equator compared to the spherically symmetric case.
2. The energy density has its minimum at the center.
3. The speed of sound is imaginary.
4. It cannot be matched to an asymptotically flat vacuum [64].

However, the Wahlquist solution can still be useful as a consistency check in case of performing a numerical study of a larger class of solutions.

6.4.2 The Kerr solution

The Kerr metric [65] describes the geometry of spacetime for the vacuum surrounding a rotating black hole. Recent studies of rotating stars, e.g. [66], indicate that the metric is not valid for describing the vacuum exterior of a more general rotating massive body, which also is in line with the conclusions in paper V. If the mass is denoted by M and the angular momentum by J, the metric can be written as

$$ds^2 = \left(1 - \frac{r_s r}{\rho^2}\right) c^2 dt^2 - \frac{\rho^2}{\Lambda^2} dr^2 - \rho^2 d\theta^2 - \left(r^2 + \alpha^2 + \frac{r_s r \alpha^2}{\rho^2} \sin^2\theta\right) d\phi^2 + \frac{2 r_s r \alpha}{\rho^2} c dt d\phi \,,$$

where $r_s = \frac{2GM}{c^2}$ is the Schwarzschild radius and

$$\alpha = \frac{J}{Mc} \,, \quad \rho^2 = r^2 + \alpha^2 \cos^2\theta \,, \quad \Lambda = r^2 - r_s r + \alpha^2 \,.$$

Some important features of the metric are that it is axisymmetric, stationary and of Petrov type D. However, there are not many candidates for matter sources of the Kerr metric with reasonable physical properties. The only known source, which was found by Neugebauer and Meinel, is shaped like a rotating disk of dust with maximal allowed angular momentum [67].

6.5 Slowly rotating stars of Petrov type D

Consider a perfect fluid model of a slowly and rigidly rotating star, where the fluid is assumed to be of Petrov type D. The fluid interior is matched to an exterior axisymmetric vacuum solution up to second order in the small rotational parameter following the Darmois-Israel procedure. Under these circumstances the Hartle form of the metric (6.1) is valid for both regions. To first order the zero-pressure surface will be unchanged from the nonrotating case, but to second order some deviation from the spherical symmetry will appear. The situation is shown in figure 6.2. Note that a prolate shape, like in the Wahlquist case, in principle would be possible unless any further restrictions are imposed. However, it turns out that asymptotic flatness excludes a prolate shape. In more detail the second order correction ξ to the zero-pressure surface can be split up in a similar way as the second order functions of the metric into a spherically symmetric part and an angular dependent part as

$$\xi(r, \theta) = \xi_0(r_1) + \xi_2(r_1) P_2(\cos\theta) \,,$$

where r_1 is the zeroth order radius. An example of the detailed structure of the matching surface can be seen in figure 6.3.

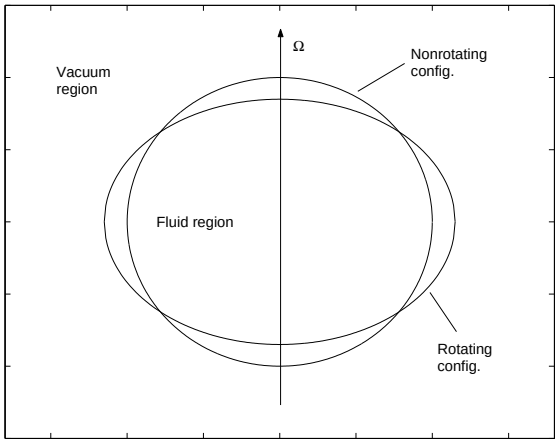

Figure 6.2: The shape of the matching surface changes from spherically symmetric to second order.

The full system consists of nine first order differential equations depending on five constants of integration corresponding to the zeroth order central pressure and energy density, the magnitude of the vorticity and two second order small constants. Moreover, a closed subsystem including six equations can be identified. The system can be solved numerically and the accuracy can be checked with the Wahlquist solution, which belongs to the considered class. Imposing the conditions of asymptotic flatness and conservation of total number of baryons determines the two second order constants of integration in terms of the zeroth and first order ones. Thus these additional constraints imply that the rotating configuration up to second order is totally determined by the zeroth order central pressure and energy density and the magnitude of the vorticity.

Figure 6.4 shows how the equation of state changes with the central pressure for some asymptotically flat solutions. Typically the energy density does not reach zero at the surface of the star, making a polytropic description

$$p = K\rho^{\gamma}\,,$$

where K and γ are constants, unrealizable. However, the polytropic index γ can be estimated close to the center to get an indication of how well the solutions in this class agree with what is known about super-compact astrophysical objects like white dwarves and neutron stars. The conclusion is that the polytropic indices are higher than the expected range of 4/3-5/3. The speed of sound is a property closely related to the equation of state calculated as $v_s^2 = \frac{dp}{d\rho}$. In order for a configuration to be physically acceptable v_s should be subluminal everywhere. Investigating this issue a range in the parameter space was found where this condition is satisfied.

Since the Kerr solution is of Petrov type D, one might think that there should exist a source for the Kerr metric within the considered class, but the numerical runs indicate that this is not the case.

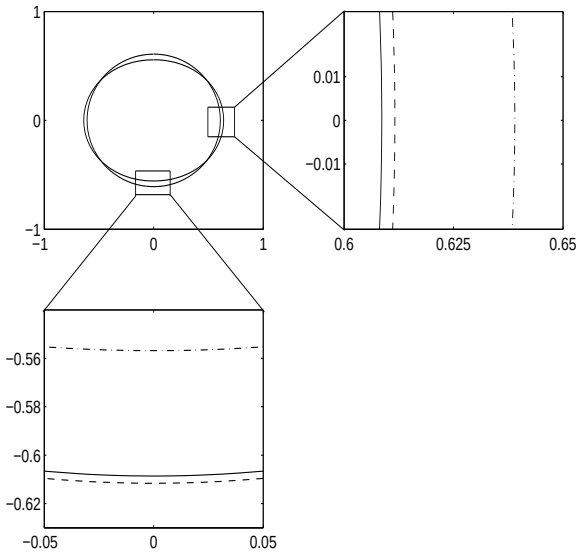

Figure 6.3: The second order corrections to the zero pressure surface using the geometric radius. The solid line in the magnified regions marks the radius of the nonrotating configuration while the dashed and dash-dotted line represent the spherically symmetric and the total second order correction respectively.

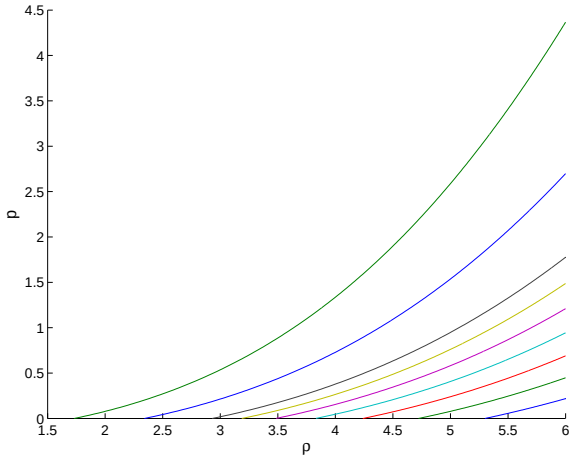

Figure 6.4: The equations of state for a sequence of values of the central pressure with the central energy density held constant.

Chapter 7

Summary of Papers

7.1 Paper I

Photon-photon scattering in vacuum due to the interaction with virtual electron-positron pairs is a phenomenon predicted by quantum electrodynamics. Even though this has been known theoretically for several decades, it is still not yet verified experimentally. In 2001 Brodin *et al.* [68] proposed a detection scheme using interacting modes in wave guides or cavities. The advantages associated with using cavities are primarily that it enables resonant interaction in a large volume and that the techniques for detecting weak signals in such confined spaces are well developed. In this paper we consider resonant three-wave interaction for two concrete cavity geometries and evaluate the corresponding coupling coefficients in terms of the quality factor of the cavity and the field strengths of the pump modes. The procedure can be summarized as follows. First the linear eigenmodes are determined and a frequency matching condition is chosen, restricting the dimensions of the cavity. Then we perform the variation of the amplitude of the eigenmodes to obtain the mode-coupling equations from the Heisenberg-Euler Lagrangian. Finally dissipation is added as a phenomenological term. The two geometries considered are a rectangular prism and a cylindrical geometry, where the latter turned out to be slightly better suited for our purposes for two reasons. The number of excited photons per unit volume is somewhat higher and if TE modes with no angular dependence are chosen, the electric field will vanish on the surfaces of the walls, eliminating the possibility of field emission. Now the only remaining restriction for the fields is the critical magnetic field, for which the superconductivity breaks down. However, there is one more important experimental complication to take into account, namely the difficulty of measuring a weak signal in the presence of other strong signals. As a possible solution to this problem we present a filtering geometry consisting of an interaction region and a filtering region having such dimensions that only the excited wave can propagate into it. The mode structure of the interaction region will be approximately unchanged by this extension of the geometry, but the mode coupling will get slightly weaker. Finite element calculations are included,

which support the feasibility of this method. Finally we discuss the possibility of non-linear currents in the walls exciting modes inside the cavity. A simple model shows that the mode coupling due to such an effect should vanish. Using performance data from current state-of-the-art superconducting niobium cavities, we conclude that the number of excited photons should be well above the detection limit.

My part in this work has been performing most of the analytic calculations of the coupling coefficients as well as the finite element calculations for the filtering geometry.

7.2 Paper II

Recent observational data consistently indicate that the expansion of the universe is accelerating and that the distribution of dark energy is time-independent. This draws attention to flat cosmological models with a cosmological constant. In this paper linear perturbations around a flat FRW universe with a cosmological constant are considered. The perturbed field equations are treated analytically, partly using a similar method as White did in the case without a cosmological constant [26]. Introducing a comoving time the equations are integrated and the complete solution is found for C^∞ perturbations and pressureless matter in terms of two elliptic integrals. It is found that there is one relatively growing and one relatively decreasing contribution to the density contrast. However, both tend to constant values in the asymptotic future. In the limit of a vanishing cosmological constant our results coincide with Sachs and Wolfe [25].

Metric perturbations along the path of a photon cause a frequency shift and thus a contribution to the temperature variation of the cosmic background radiation called the Sachs-Wolfe effect. The temperature variations associated with the considered metric perturbations are calculated using the method of Sachs and Wolfe. We conclude that for the relatively increasing mode the CMBR power spectrum is attenuated by an overall factor 3 in the presence of a cosmological constant, which is in good agreement with numerical results by Hu and Sugiyama [69].

I have contributed to this work by participating in the integration of the perturbed field equations.

7.3 Paper III

Judging by the existence in literature on exact solutions, it has proven to be very difficult to find cosmological perfect fluid models with both non-zero expansion and vorticity. In this paper we consider cosmological models of Bianchi type V and I containing a perfect fluid with a linear equation of state and a cosmological constant. This class is known to contain solutions with a rotating matter flow. The method used for contructing solutions within this class is based on a theorem by Cartan saying that a geometry is locally completely determined by a set, R^{p+1}, containing the Riemann tensor and a finite

number of its covariant derivatives. Starting out by specifying this set, we impose certain integrability conditions equivalent to the Ricci identities in order for the set to describe a geometry. In the case of symmetries some additional integrability conditions are needed, namely parts of the cyclic and Bianchi identities. Without symmetries it is possible to solve for all the 1-forms to get the full line-element, but otherwise the Lie-algebra of the isometry group has to be determined, from which an ansatz for the remaining 1-forms can be made. Calculating R^{p+1} from the ansatz and comparing with the initial configuration determines the validity of the result. The main advantages are that the approach is coordinate invariant and that the elements in R^{p+1} correspond to directly measurable quantities, making physical requirements easy to impose.

In the case of Bianchi type V the method produces a general system which can be reduced to five first order differential equations plus four algebraic constraints and the full line-element can be found in terms of quadratures, given that the system of ODEs is solved. Moreover, a first order perturbation around the open Friedmann universe is considered. The linearized equations can be completely integrated for the dust and radiation case. It is possible to express the second order perturbations as quadratures, but this is not done explicitly in this work. The equations for the perturbations of the tilt are special in the sense that they decouple from other quantities of the same order. A number of important subcases like orthogonal solutions and irrotational tilted solutions are considered. Finally a numerical study of the general system is performed using the Runge-Kutta method with a fourth order truncation error with respect to the step length. For appropriate initial vaues the numerical solution agrees well with the perturbative calculation and there is a clear convergence for the tilt when including the second order term. The asymptotic behaviour is investigated numerically as well, showing good agreement with previous results for late times obtained through dynamical system analysis [40].

The authors have cooperated in performing the calculations throughout this article. I have also written most of the source code used for the numerical solutions.

7.4 Paper IV

The gravitational interaction between electromagnetic waves is investigated at the single photon level using a general relativistic treatment. The interaction is caused by the curvature of space-time associated with the presence of the waves themselves. In particular, the problem of finding the coupling equations and cross-section for photon-photon scattering, i.e. four-wave interaction, is handled with a perturbative approach to the classical Einstein-Maxwell system. This is interesting both as a comparison with results obtained for graviton mediated photon-photon scattering using QFT methods and also to determine the importance of the gravitational interaction in relation to other photon-photon scattering processes, e.g. due to exchange of virtual electron-positron pairs. The cross-section coincides with its QFT counterpart in the limit of small scattering angles, but

for larger angles there is a clear deviation, possibly originiating from shortcomings in the procedure to obtain the interaction potential from the matrix scattering amplitude in the QFT case [18]. The relatively weak frequency dependence of the gravitational interaction makes it important in the low frequency regime, even though the scattering via virtual electron-positron pairs is dominating in a major part of the frequency spectrum. The significance of the two contributions become comparable at $\omega \sim 30$ rad/s.

My part in this work has been deriving the coupling equations and the cross-section as well as writing most of section II of the manuscript.

7.5 Paper V

The Hartle formalism is used to study perfect fluid models of slowly and rigidly rotating stars perturbatively up to second order in the small rotational parameter. A Petrov type D condition is used for the fluid instead of an explicit equation of state to close the system. The choice of Petrov type is motivated by the fact that this is the only algebraically special class possibly containing physically interesting solutions. The fluid is matched to an exterior stationary and axisymmetric vacuum solution at the zero-pressure surface, which has a non-spherical shape to second order. It is found that this matching can be done up to second order for all solutions in the considered class, irrespective of Petrov type. The interior configuration is governed by a system of nine first order differential equations depending on five constants of integration. A closed subsystem consisting of six ODEs is solved numerically using the fourth order Runge-Kutta method and the special case of the analytic Wahlquist solution provides an accuracy check. Requiring asymptotic flatness for the vacuum exterior reduces the dimension of the parameter space from five to four, leaving the closed subsystem fully determined by the zeroth order central pressure and energy density and the magnitude of the vorticity. Moreover, the equation of state and speed of sound is determined for some asymptotically flat solutions and a range in the parameter space is found where the speed of sound is subluminal. An important conclusion based on the numerical study is that no source for the Kerr metric to second order can be found among these Petrov type D fluids.

My contribution here is mainly in the numerical part, but I have also been involved in the problem of matching the metrics.

7.6 Paper VI

Here the prerequisites are the same as in paper V. The full system of equations is solved numerically with emphasis on those not being part of the closed subsystem. These equations determine the total number of baryons and the mass shift of the star and also hold the necessary information for plotting the zero-pressure surface to second order. Requiring that the total number of baryons should be unchanged by the rotation in addition

to the previous condition of asymptotic flatness reduces the number of free parameters one step further, resulting in a situation where the rotating configuration up to second order is completely determined by the zeroth order central pressure and density and the magnitude of the vorticity. The mass shift, which is a combined effect of the change in gravitational potential energy and rotational kinetic energy, is found for a sequence of solutions. Finally, the scaling invariances of the closed subsystem are used to investigate the dependence of the second order corrections to the zero-pressure surface on the angular velocity of the fluid region with respect to a distant stationary observer.

Acknowledgements

First of all I would like to thank my supervisor Michael Bradley for invaluable support during these years. Then I want to thank my family and my grandfather for their equally important support outside the field of physics. Moreover, I am grateful for the collaboration with Gert Brodin and Mattias Marklund. I would also like to thank my colleagues at the KFKI research institute in Budapest Mátyás Vasúth, Viktor Czinner, István Rácz, Gyula Fodor and the late Zoltán Perjés. Finally, many thanks to my roommates at the department.

Bibliography

[1] http://lisa.jpl.nasa.gov

[2] http://www.ego-gw.it/virgodescription/pag_4.html

[3] http://www.ligo.caltech.edu/advLIGO/

[4] Ellis G.F.R. and Van Elst H. (1999) Cargèse Lectures, *Theoretical and Observational Cosmology*, Ed. M. Lachièze-Rey, Kluwer Academic Publishers, Netherlands

[5] Feynman R.P. and Hibbs A.R. (1965) *Quantum Mechanics and Path Integrals*, McGraw-Hill, New York

[6] Dittrich W. and Gies H. (2000) *Probing the quantum vacuum*, Springer

[7] Barker B.M., Bathia M.S. and Gupta S.N. (1967) *Phys. Rev.* **158**, 1498

[8] Itzykson C. and Zuber J.B. (1985) *Quantum Field Theory*, McGraw-Hill Book Co., Singapore

[9] Dewar R.L. (1974) *Phys. Rev. A* **10**, 2017

[10] Alexandrov E.B., Anselm A.A. and Moskalev A.N. (1985) *Zh. Eksp. Teor. Fiz.* **89**, 1181 [(1985) *Sov. Phys. JETP* **62**, 680]

[11] Ding Y.J. and Kaplan A.E. (1989) *Phys. Rev. Lett.* **63**, 2725

[12] Rozanov N.N. (1993) *Zh. Eksp. Teor. Fiz.* **103**, 1996 [(1998) *J. Exp. Theor. Phys.* **76**, 991]

[13] Rozanov N.N. (1998) *Zh. Eksp. Teor. Fiz.* **113**, 513 [(1998) *J. Exp. Theor. Phys.* **86**, 284]

[14] Ding Y.J. and Kaplan J. (1992) *J. Nonlinear Opt. Phys. Mater* **1**, 51

[15] Soljacic M. and Segev M. (2000) *Phys. Rev. A* **62**, 043817

[16] Shen B., Yu M.Y. and Wang X. (2003) *Phys. Plasmas* **10**, 4570

[17] Kaplan A.E. and Ding Y.J. (2000) *Phys. Rev. A* **62**, 043805

[18] Kazakov K.A. (2001) *Class. Quantum Grav.* **18**, 1039

[19] Brattke S., Varcoe B.T.H. and Walther H. (2001) *Phys. Rev. Lett* **86**, 3534

[20] Nogues G. *et al.* (1999) *Nature (London)* **400**, 239

[21] Cartan E. (1946) *Leçons sur la Geometrie des Espaces de Riemann*, Gauthier-Villars.

[22] Karlhede A. (1980) *Gen. Relativ. Gravit.* **12**, 693

[23] Bradley M. and Marklund M. (1996) *Class. Quantum Grav.* **13**, 3021

[24] Foster J. and Nightingale J.D. (1995) *A short course in general relativity*, Springer

[25] Sachs R.K. and Wolfe A.M. (1966) *ApJ* **147**, 73

[26] White P.C. (1973) *J. Math. Phys.* Vol. **14**, 831

[27] Ellis G.F.R. and MacCallum M.A.H (1969) *Commun. Math. Phys.* **12**, 108

[28] Armendariz-Picon C., Mukhanov V. and Steinhardt P.J. (2000) *Phys. Rev. Lett.* **85**, 4438

[29] Barrett R.K. and Clarkson C.A. (2000) *Class. Quantum Grav.* **17**, 5047

[30] Tonry J.L., Schmidt B.P., Barris B. *et. al.* (2003) *Astrophys. J.* **594**, 1

[31] Conley A. *et al.* (2006) *Astrophys. J.* **644**, 1

[32] Spergel D.N. *et al.* (2007) *Astrophys. J. Suppl. Series* **170**, 377

[33] Tegmark M., Strauss M.A. and Blanton M.R. *et al.* (2004) *Phys. Rev. D* **69**, 103501

[34] Gödel K. (1949) *Rev. Mod. Phys.* **21**, 447

[35] Rosquist K. (1983) *Phys. Lett.* **97A**, 145

[36] Clemence C.M. (1957) *Rev. Mod. Phys.* **29**, 2

[37] Hawking S. (1969) *Mon. Not. R. Astr. Soc.* **142**, 129

[38] Collins C.B. and Hawking S. (1973) *Mon. Not. R. Astr. Soc.* **162**, 307

[39] Collins C.B. and Ellis G.F.R (1979) *Phys. Rep.* **56**, 65

[40] Coley A. and Hervik A. (2005) *Class. Quantum Grav.* **22**, 597

[41] Thirring H. (1918) *Phys. Zs.* **19**, 33

[42] Lense J. and Thirring H. (1918) *Phys. Zs.* **19**, 156

[43] http://www.nasa.gov/mission_pages/gpb/index.html

[44] Friedman J.L. and Ipser J.R. (1992) *Philos. Trans. R. Soc. London, Ser. A* **340**, 391

[45] Butterworth E.M. and Ipser J.R. (1976) *Astrophys. J.* **204**, 200

[46] Komatsu H., Eriguchi Y. and Hachisu I. (1989) *Mon. Not. R. Astron. Soc.* **237**, 355

[47] Komatsu H., Eriguchi Y. and Hachisu I. (1989) *Mon. Not. R. Astron. Soc.* **239**, 153

[48] Neugebauer G. and Herold H., *Lecture Notes in Physics* **410**, 305 (Springer, Berlin, 1992)

[49] Bonazzola S., Gourgoulhon E. and Marck J.A. (1998) *Phys. Rev. D* **58**, 104020

[50] Bonazzola S., Gourgoulhon E., Salgado M. and Marck J.A. (1993) *Astron. Astrophys.* **278**, 421

[51] Ansorg M., Kleinwächter A. and Meinel R. (2002) *Astron. Astrophys.* **381**, L49

[52] Stergioulas N. (2003) *Living Rev. Relativity* **6**, 3, http://www.livingreviews.org/lrr-2003-3

[53] Hartle J.B. (1967) *Astrophys. J.* **150**, 1005

[54] Cutler C. and Lindblom L. (1987) *Astrophys. J.* **314**, 234

[55] Flowers E. and Itoh N. (1976) *Astrophys. J.* **206**, 218

[56] Flowers E. and Itoh N. (1979) *Astrophys. J.* **230**, 847

[57] Hegyi D.J. (1977) *Astrophys. J.* **217**, 244

[58] Shapiro S.L. (2000) *Astrophys. J.* **544**, 397

[59] Darmois G. (1927) in *Mémorial de Sciences Mathématiques*, **XXV**, Chap. V

[60] Israel W. (1966) *Il Nuovo Cimento* **BXLIV** 4348

[61] Perjés Z. and Vasúth M. (2003) *Class. Quantum Grav.* **20**, 5241

[62] Fodor G. and Perjés Z. (2000) *Gen. Relativ. Gravit.* **32**, 2319

[63] Wahlquist H.D. (1968) *Phys. Rev.* **172**, 1291

[64] Bradley M., Fodor G., Marklund M. and Perjés Z. (2000) *Class. Quantum Grav.* **17**, 351

[65] Kerr R.P. (1963) *Phys. Rev. Lett.* **11**, 237

[66] Berti E., White F., Maniopoulou A. and Bruni M. (2005) *Mon. Not. R. Astron. Soc.* **358**, 923

[67] Neugebauer G. and Meinel R. (1993) *Astrophys. J.* **414**, L97

[68] Brodin G., Marklund M. and Stenflo L. (2001) *Phys. Rev. Lett.* **87**, 171801

[69] Hu W. and Sugiyama N. (1995) *Phys. Rev. D* **51**, 2599